Agricultural and Forest Meteorology 353 (2024) 110061

Contents lists available at ScienceDirect

Agricultural and Forest Meteorology

journal homepage: www.elsevier.com/locate/agrformet

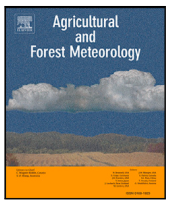

Thinning turned boreal forest to a temporary carbon source - short term effects of partial harvest on carbon dioxide and water vapor fluxes

Toprak Aslan [a,d,*], Samuli Launiainen [b], Pasi Kolari [a], Olli Peltola [b], Juho Aalto [c], Jaana Bäck [c], Timo Vesala [a,c], Ivan Mammarella [a]

[a] Institute for Atmospheric and Earth System Research (INAR)/Physics, Faculty of Science, P.O. Box 64, Helsinki, 00014, Finland
[b] Natural Resources Institute Finland (Luke), Latokartanonkaari 9, Helsinki, 00790, Finland
[c] Institute for Atmospheric and Earth System Research (INAR), Forest Sciences, P.O. Box 27, Helsinki, 00014, Finland
[d] Finnish Meteorological Institute, P.O. Box 503, Helsinki, 00101, Finland

ARTICLE INFO

Dataset link: https://doi.org/10.23729/b4575245-5612-4874-a33b-541b215b1a10, https://doi.org/10.23729/23dd00b2-b9d7-467a-9cee-b4a122486039, https://smear.avaa.csc.fi/, https://b2share.eudat.eu/records/e027118ea22148ef92789e740116711e

Keywords:
Eddy covariance
Net ecosystem exchange
Even-aged forestry
Thinning
Boreal forest

ABSTRACT

Even though the effect of thinning on CO_2 and H_2O fluxes has been widely investigated, a holistic description of thinning-induced responses is yet to be provided. Here, we present a comprehensive study, investigating the impact of commercial thinning in an even-aged boreal forest in southern Finland using concurrent above- and sub-canopy eddy-covariance measurements and a process-based ecosystem model. The thinning was done from below and removed ca. 40% of the basal area. The forest turned from a strong sink (-271 $gCm^{-2}yr^{-1}$) to a moderate carbon source ($+115$ $gCm^{-2}yr^{-1}$) during the year of thinning due to decreased ecosystem gross primary productivity (GPP_{eco}) and simultaneous increase in ecosystem respiration (R_{eco}). The reduced canopy density increased the light availability, near-ground air temperature and wind speed. This improved the photosynthetic efficiency of the remaining trees, resulting in only a moderate reduction in GPP_{eco} (ca. 20%) compared to the foliage loss (ca. 45%). The decomposition of cutting residue likely increased the heterotrophic respiration that compensated for the reduced autotrophic respiration of removed trees, leading to R_{eco} exceeding long-term average by ca. 10% during the year of thinning. Interestingly, thinning did not affect ecosystem evapotranspiration but changed its partitioning: both stand transpiration and interception evaporation decreased, whereas forest floor evapotranspiration increased. The inter-annual weather variability did not notably affect annual fluxes, which enabled robust quantification of thinning impacts. Our results show a strong qualitative resemblance with previously reported short-term responses of boreal forest to thinning. This is presumably due to similar management practices and species composition among the studies, and low variability of inter-annual weather and fluxes. Our study showed that sub-canopy eddy covariance measurements and process-based model can play a pivotal role in disentangling the confounding responses of forest floor and canopy to thinning.

1. Introduction

Forests offset a large fraction of anthropogenic greenhouse gas emissions (Pan et al., 2011; Friedlingstein et al., 2019), regulate the global water cycle (Gerten et al., 2004; Schlesinger and Jasechko, 2014), and provide wood, biomass, wealth, and well-being for the societies (Miura et al., 2015; Brockerhoff et al., 2017; Kellomäki, 2022). Boreal forests spatially constitute one-third of global forests (Keenan et al., 2015) and contribute ca. 22% of global forest carbon sink (Pan et al., 2011). In Northern Europe, the majority of boreal forests are managed for wood production via even-aged forestry (EAF) (Kuuluvainen et al., 2012; Kellomäki, 2022). A typical EAF management regime consists of an initial stand establishment with native coniferous species (Scots pine and Norway spruce), a pre-commercial thinning at the age of 10–15 years, and two or three commercial thinnings, and a final felling at the end of the 60–100 year rotation period (Kellomäki, 2022). Forest thinning is a partial stand harvest designed to reduce between-tree competition and allocate growth resources (e.g. light, water, nutrients) to the remaining trees, enhance their vitality and growth to maximize economic income over the rotation period (Kellomäki, 2022).

Recently, forest ecosystems and their management have acquired an increasing interest considering their potential to mitigate climate change (Canadell and Raupach, 2008; Bonan, 2008; Lemprière et al.,

* Corresponding author at: Finnish Meteorological Institute, P.O. Box 503, Helsinki, 00101, Finland.
E-mail address: toprak.aslan@fmi.fi (T. Aslan).

https://doi.org/10.1016/j.agrformet.2024.110061
Received 21 November 2023; Received in revised form 1 April 2024; Accepted 13 May 2024
Available online 22 May 2024
0168-1923/© 2024 The Author(s). Published by Elsevier B.V. This is an open access article under the CC BY license (http://creativecommons.org/licenses/by/4.0/).

2013). There is also a strong demand to adapt forest management to the changing climate (Lindner et al., 2014; Keenan, 2015; Venäläinen et al., 2020), and provide biodiversity conservation by, for instance, moving towards continuous-cover forestry based on frequent selection harvests (Pukkala et al., 2011; Peura et al., 2018). Together, these now require a renewed focus on the biogeophysical and biogeochemical effects of thinning, in particular its effect on short-term carbon sequestration and emissions (Vesala et al., 2005; Lindroth et al., 2020), water cycle (Leppä et al., 2020; Lagergren et al., 2008; del Campo et al., 2022; Laurent et al., 2003) and local microclimates (Aussenac, 2000; Ma et al., 2010).

Earlier thinning studies have reported contrasting short-term (i.e. 1–4 post-harvest years) responses on the net ecosystem exchange of carbon (NEE). Vesala et al. (2005) observed a proportional reduction in gross photosynthetic productivity (GPP) and ecosystem respiration (R), resulting in no change in NEE. Dore et al. (2010), Saunders et al. (2012) and Lindroth et al. (2018) reported a greater reduction in GPP than in R, resulting in decreasing carbon sequestration ability. Wilkinson et al. (2016) showed no significant change in any components of carbon fluxes. It is expected (Duursma and Mäkelä, 2007) and often reported that ecosystem GPP decreases less than the rate of foliage loss (Vesala et al., 2005; Saunders et al., 2012; Wilkinson et al., 2016). This is mainly attributed to the compensation by the thriving remaining trees and ground vegetation due to the increasing resource availability and decreasing competition. The magnitude of the compensation however remains inconclusive as the change in microclimatic conditions in trunk space and at the forest floor depends on first the initial stage of the forest (species composition, leaf area index - LAI) and then the application of the thinning (intensity, i.e. the fraction of biomass removed).

As for R, the effect of the decomposition of easily degradable thinning-induced materials (i.e., fine roots, cutting residues, and needles) plays an important role in varying responses. Accordingly, the expected response is that R would increase because of the contribution of enhanced decomposition (Vesala et al., 2005; Wilkinson et al., 2016). However, as autotrophic (R_a) and heterotrophic (R_h) respiration relate to different biological processes that may respond differently to the thinning, the response of their sum (i.e. R) on the thinning can be complex.

Similar to NEE, the responses of evapotranspiration (ET) have varied. Many studies report no change in ET with a reduction in transpiration (T) (Vesala et al., 2005; Lagergren et al., 2008), an increase in ET with a reduction in T (Skubel et al., 2017), whereas some reported a reduction in ET (Dore et al., 2010). As the biological component of ET, the reduction in T is expected to be similar to GPP. Evaporation (E), however, depends more on weather conditions and the distribution of water within forest layers. It is well known that thinning reduces canopy interception (Heikurainen et al., 1970; Cheng et al., 2020; McJannet and Vertessy, 2001; Crockford and Richardson, 2000) increasing the amount of water reaching the forest floor. This then leads to decreasing canopy evaporation, increasing forest floor evaporation (often associated with better ventilation and light conditions), and soil water availability. Due to various counteracting processes within and between different layers, quantifying the responses of T and E to thinning is challenging.

One of the most common ways to monitor stand – atmosphere carbon and water fluxes is the eddy covariance technique (EC) (Baldocchi, 2008). EC flux measurements however are typically conducted only above the canopy, providing the integrated response of the ecosystem. Estimating the separate contribution of the canopy and forest floor layers requires complementary approaches, such as carbon budgeting (Aun et al., 2021), upscaling of chamber measurements (Kolari et al., 2006), sub-canopy EC (Lindroth et al., 2018; Launiainen et al., 2005; Paul-Limoges et al., 2017; Thomas et al., 2013) or process-models (Pinnington et al., 2017; Leppä et al., 2020). However, to our knowledge, there is no thinning study incorporating these approaches in a single experiment. This is urgently needed to understand the role of component fluxes from different layers for a holistic description of thinning-induced responses.

We present here a comprehensive case study designed to assess thinning-induced changes in carbon and water fluxes in a boreal coniferous forest in southern Finland. We used concurrent above and sub-canopy EC measurements, and automatic chamber measurements as well as a process-based model to determine the short-term responses to commercial thinning. With these tools, we address the following hypotheses; (H1) GPP would decrease due to foliage reduction with a smaller magnitude compared to that of the foliage loss, (H2) R would decrease, but to a lesser extent because of the contribution of decomposition of cutting residues and fine roots, and (H3) as a result of GPP and R responses, the net carbon uptake would decrease, however the forest would still remain as a sink of carbon after thinning. Regarding water fluxes, we hypothesize that (H4) forest floor E and T increase, whereas canopy T decreases. Therefore, (H5) ecosystem level ET would decrease relative to pre-thinning values as canopy T is often recognized as the major component of ET in boreal forests.

2. Materials and methods

2.1. Study site and thinning

The study site, namely Hyytiälä SMEAR II, is located in southern Finland (61°51′N,24°17′E, 81 m above sea level) and represents a typical Scots pine (*Pinus sylvestris* L.) dominated mesic/sub-xeric boreal coniferous stand, established by sowing after prescribed burning conducted in 1962. In addition to Scots pine, self-regenerated Norway spruce (*Picea abies* (L.) Karst), birches (*Betula sp.*), and some individuals of other deciduous species (e.g. *Populus tremula*, *Sorbus aucuparia*) were growing at the site. The forest stands within a 200 m radii surrounding the above-canopy EC tower (EC_{eco}) have been mostly outside of routine forest management, with the exception of partial thinning of the northern sector in the early 1990s, and a mild thinning of the southern sector in 2002 (Vesala et al., 2005). In 2018, the majority of the stand within the 200 m radii were rather dense and the ratio between the living crown and tree height started to decrease, and some self-thinning already took place in parts of the forest. Most of the stands located farther than 200 m away from EC_{eco} have been managed by Metsähallitus (State Forests) following typical guidelines for EAF in Finland (Kolari et al., 2022).

The thinning was conducted in two phases, i.e., understorey removal (UR), and main harvest (MH) via following the same guidelines as recommended for a stand in such development stage (Yrjölä, 2002; Kellomäki, 2022). Here on, the term ‘‘thinning’’ is used to describe the combined effect of UR and MH to be analyzed in this study. Correspondingly, the year 2019 is associated with the changes due to UR, 2020 due to MH, and 2021 and 2022 are identified as first and second post-thinning year, respectively. In the spring of 2019, the majority of small and non-commercial trees with a diameter at breast height (DBH) of less than 7 cm were manually felled with a brush saw. Only juniper (*Juniperus communis* L.) was left to grow. The felled understorey trees were left on site. MH took place in February–March 2020 using forest harvesters and forwarders, with the exception of ca. one-hectare area close to the measurement infrastructure that was thinned manually already in December 2019 and January 2020. Wintertime was chosen in order to minimize root damage caused by heavy machines. The cutting residues, including stumps, root system, needles, branches, and upper non-valuable crowns were left at the site as is typically done in Finland.

Allometric measurements were conducted at 43 measurement plots spanning over the area with 400 m radii around EC_{eco} (Aalto et al., 2023). However, in this study, we only focus on the data within 200 m radii excluding the sector 105–190° for compatibility of the spatial extent of thinning and the source area of EC_{eco} (Fig. 1a).

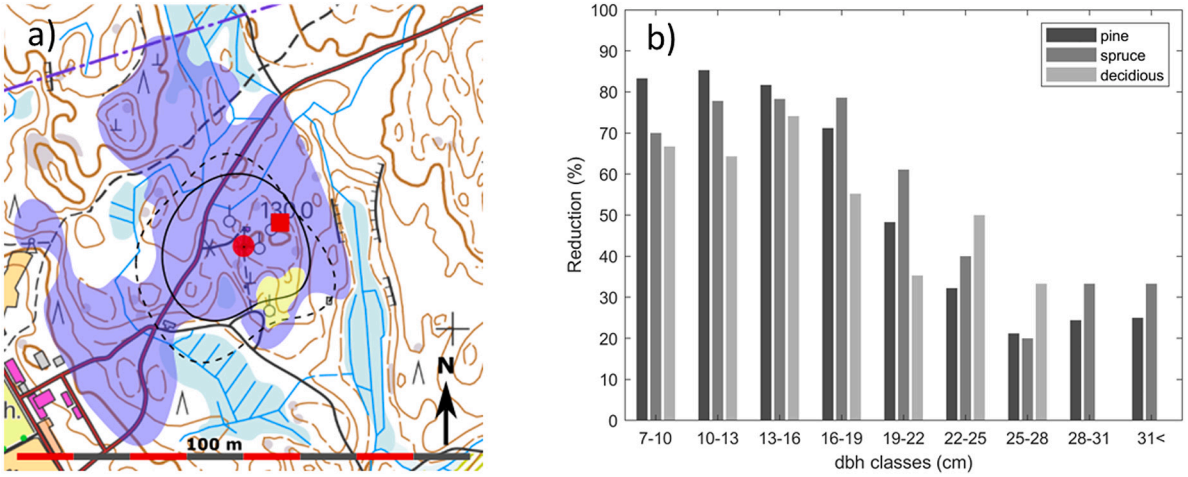

Fig. 1. (a) Map of the site overlaid with the harvesting area highlighted with blue color and a control area (not included in the analysis) shown with yellow color (see Section 2.1). The location of the above-canopy EC mast (EC_{eco}) is marked with a circle, and the below-canopy EC mast (EC_{ff}) with a square. The black-solid line shows the daytime source area of EC_{eco}, while the black-dashed line shows the nighttime (Appendix B). (b) The fraction of removed trees during the main harvest (MH) in 2020 relative to the intact forests (%) for different tree species with respect to their diameter at breast height (DBH).

During MH, mostly suppressed or sub-dominant trees were cut for the majority of the area, with only a few exceptions of co-dominant or dominant trees. Consequently, the relative reduction of tree species (i.e., Scots pine, spruce, and deciduous) decreased with increasing DBH (Fig. 1b). The parts of the stand that did not require thinning (already sparse enough and will not need commercial thinning within the next 10 years) were left untouched, resulting in a non-uniform harvesting area (shown with blue in Fig. 1a).

In total, about 80% of the forest area (about 12.5 ha) within a 200 m radius from EC_{eco}, as well as 10 ha outside of the 200 m radius was thinned (Fig. 1a). Together UR and MH decreased stand basal area (BA, m^2 ha^{-1}) by ca. 40%, one-sided LAI (see Section 2.2.5) by ca. 45% and stem density by ca. 60% (Table 1). In total 3.9 kg C m^{-2} of living tree biomass was harvested, of which 62% (2.4 kg C m^{-2}) was commercial removal as logs and pulpwood, whereas 38% (1.5 kg C m^{-2}) was left on site as cutting residues. The initial species composition was approximately maintained. The thinning ratio (TR), defined as the ratio of the mean BA of harvested and remaining trees, was 0.04 for UR and 0.61 for MH. This is classified as a low thinning causing negligible effect on dominant canopy height (ca. 23 m). LAI slightly increased from 2.1 to 2.2 and then 2.5 in 2021 and 2022, respectively.

A small area ca. 0.75 ha (the yellow patch in Fig. 1a) was left intact to ensure that there is a suitable control area for follow-up studies comparing the effects of thinning on needle, tree, and soil plot level processes. The fluxes originating from this area were not included in EC data (Section 2.2.1).

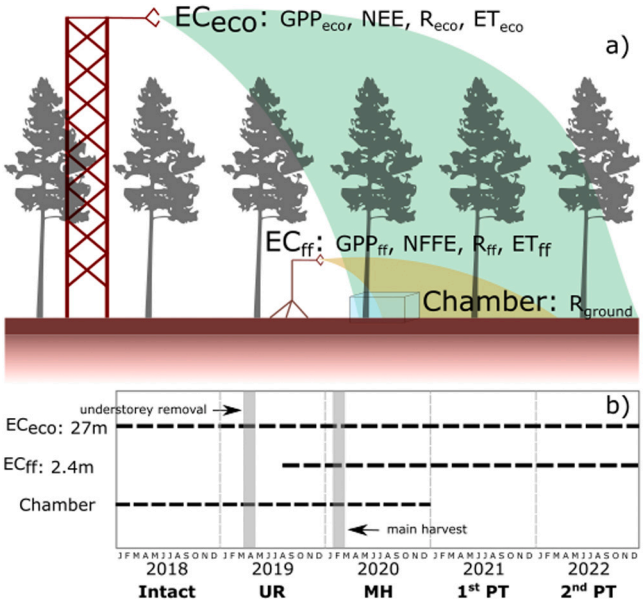

Fig. 2. (a) Measurement setups. Eddy covariance (EC) setup located above the canopy is denoted with "eco", measures ecosystem fluxes, whereas below canopy setup (EC_{ff}) detects forest floor fluxes. Chamber measurements represent ground fluxes. (b) Data coverage and timing of understorey removal (UR, April-May 2019) and the main harvest (MH, January-February 2020). The 2018 represents intact forest, 2019 and 2020 disturbance years (UR and MH, respectively), while 2021 and 2022 first and second post-thinning (PT) years, respectively.

2.2. Measurements and data processing

2.2.1. EC measurements

The fluxes of CO_2 and H_2O were concurrently measured with eddy-covariance above the forest (EC_{eco}) at 27 m height and below (EC_{ff}, forest floor fluxes) the forest canopy at 2.4 m height (Fig. 2). EC_{eco} observed ecosystem level fluxes, i.e. NEE and ET_{eco}, while EC_{ff} measured forest floor fluxes, i.e., net forest floor exchange (NFFE) and forest floor evapotranspiration (ET_{ff}). The EC_{eco} system is part of the Integrated Carbon Observation System (ICOS, site-code FI-Hyy) Ecosystem Station network (Franz et al., 2018; Heiskanen et al., 2022), which officially started in March 2018. EC_{ff} measurements started in August 2019. EC_{ff} is located ca. 100 m away from EC_{eco} setup in ENE direction with negligible elevation difference (Fig. 1a).

EC_{eco} includes an enclosed-path nondispersive infrared sensor (LI-7200, LI-COR Biosciences, USA) for measuring CO_2 and H_2O dry mole fractions and an ultrasonic three-dimensional anemometer (HS-50, Gill Ltd, UK) for measuring three wind velocity components and sonic temperature at 10 Hz frequency. Gas was sampled with a heated LI-COR sample tube (length 0.67 m, internal diameter 6 mm) at 12 LPM flow rate. The configuration of measurement setup was according to ICOS recommendations (Rebmann et al., 2018).

EC_{ff} consists of an enclosed-path nondispersive infrared sensor (LI-7200, LI-COR Biosciences, USA) and an ultrasonic three-dimensional anemometer (model USA-1; METEK GmbH, Elmshorn, Germany). Gas sampling was done via Eaton Synflex tube with a 6 mm diameter (length 0.35 m) and 12.5 mm diameter (length 1.67 m) at a 12 LPM flow rate.

We used the EddyUH software (Mammarella et al., 2016) to process both the above and below canopy EC raw data and to compute the 30 min average fluxes according to the ICOS protocol (Sabbatini et al., 2018). Briefly, we performed standard data processing steps, such as the raw data despiking, double rotation of the coordinate system reporting the wind velocity components and time-lag correction via cross-covariance maximization. Flux underestimation at low-frequency was corrected via Rannik and Vesala (1999), while the one at high-frequency was corrected via experimental transfer functions for gas fluxes (Mammarella et al., 2009) and theoretical transfer functions for momentum and sensible heat flux (Moncrieff et al., 1997).

EC fluxes were further screened using criteria for stationarity, and the skewness and the kurtosis of vertical wind speed and the mixing ratios during the 30-min averaging period (Foken and Wichura, 1996). Above-canopy fluxes measured at wind direction between 130 and 190 deg were rejected due to a contribution of the unthinned control area and possible flow distortion caused by the flux tower (Fig. 1a). We assumed that the fluxes of EC_{eco} originated from the thinned area, and correspondingly applied no footprint-related filtering (see Appendix B for more details). Fluxes in low light (nighttime) were screened with friction velocity (u_*) thresholds of 0.37 m s^{-1} (2018–19) and 0.42 m s^{-1} (2020–22) for EC_{eco}, while with the standard deviation of vertical wind speed threshold of 0.08 m s^{-1} for sub-canopy fluxes (Launiainen et al., 2005). Unstable conditions (Obukhov length, L >−1000 and <0 m) were required for daytime fluxes.

Both above- and below-canopy EC fluxes were corrected for storage change under the EC measurement height using air temperature and gas concentrations measured at several heights at the EC_{eco} flux tower according to ICOS protocol (Montagnani et al., 2018).

ET fluxes were gapfilled with marginal distribution sampling method (Wutzler et al., 2018), utilizing a combination of mean diurnal variation of fluxes and look-up tables with the measure of global radiation (R_g), air temperature, and vapor pressure deficit (VPD). Net carbon fluxes (NEE and NFFE) were gap-filled and partitioned into photosynthesis (GPP_{eco} and GPP_{ff}) and respiration (R_{eco} and R_{ff}) using empirical regressions fitted to good-quality fluxes (see Appendix C).

Additional estimates of annual NEE were also produced with the marginal distribution sampling, and component fluxes with REddyProc software (Wutzler et al., 2018) to assess the uncertainty stemming from gapfilling and partitioning procedures. This assessment is presented in Appendix C.

In this study, we followed micrometeorological sign convention where negative NEE indicates net carbon uptake (NEE = -GPP + R).

2.2.2. Evapotranspiration partitioning and water-use efficiency

We partitioned tree canopy transpiration (T_{stand}) from ET_{eco} using the concurrent EC setups following Paul-Limoges et al. (2020) (here on EPL20). The EPL20 estimates T_{stand} as the difference between ET_{eco} and ET_{ff} when certain conditions are met. To do so, we first discarded rainy periods from both ET_{eco} and ET_{ff} and removed negative ET values (condensation) from ET_{ff} in addition to periods when below canopy air temperature was below dew point temperature. Unlike EPL20, we did not gap-fill discarded periods as we only present the ratio of T_{stand} and ET_{eco}, not the seasonal budget. We computed ecosystem water use efficiency (WUE_{eco}) as the slope of the relationship between monthly median GPP_{eco} and ET_{eco} during the growing season calculated from not gapfilled time series. We define the annual period as the calendar year, while growing season is the period between May 1st and October 31st.

2.2.3. Separating the effects of inter-annual weather variability and thinning on annual fluxes

To separate the effect of inter-annual weather variability (IAWV) and thinning, we used a simple approach to model CO_2 fluxes, similar to Hadden and Grelle (2016). We used the median of flux partitioning model parameters (Appendix C) of R_{eco} and GPP_{eco} for 2009–2017, representing intact forest with the considerably normal weather condition, with the weather data of 2019 (representing UR) and 2020 (representing MH).

Table 1
Characteristic of the study site before and after understorey removal (UR) and main harvest (MH). The coarse-cutting residue consists of branches, stumps, and coarse roots (>1 cm) while fine-cutting residue includes needles and leaves.

	2018 (intact)	2019 (UR)	2020 (MH)
Stems DBH ≥ 7 cm (ha^{-1})	1141	969	465
Basal area DBH ≥ 7 cm (m^2 ha^{-1})	30.7	30.4	18
One-sided tree LAI (m^2 m^{-2})	3.9	3.6	2.1
Coarse-cutting residue (g C m^{-2})	–	514	871
Fine-cutting residue (g C m^{-2})	–	43	80
Total cutting residue (g C m^{-2})	–	557	951

2.2.4. Chamber measurements

Ground CO_2 efflux (R_{ground}), consisting of soil heterotrophic and root and ground-vegetation autotrophic respiration, was measured with two automatic chambers in 2018–2019, while with three in 2020 during snow-free periods. The chambers (20 cm × 20 cm × 25 cm) were made of 6-mm-thick acrylic and were positioned on aluminum frames (7 cm in height). The frames were inserted into the litter layer of the soil. The chambers were covered with aluminum foil to exclude light when the chamber was closed. CO_2 concentration inside the chambers was recorded with a GMP343 diffusion type CO_2 probe (Vaisala Oyj, Vantaa, Finland), which has a measurement range of 0 to 1000 ppm. The chambers were closed for 3.5 min every 30 min, recording the concentration at 5-s intervals. The CO_2 efflux was calculated by linear fitting of time vs. temperature-, pressure- and humidity-corrected CO_2 concentration records taken 40..180 s from the chamber closing. The measurements are detailed in Pumpanen et al. (2015).

2.2.5. Auxiliary measurements

We used long-term (2009–2017) EC_{eco} data to compute average annual pre-thinning fluxes of CO_2 and H_2O (Launiainen et al., 2022). In addition, we used the same data set to complement the EC_{eco} flux data for the first three months of 2018.

Photosynthetically active radiation (PAR) was measured at (1) below canopy at 0.6 m height (PAR_{ff}) via an array of four sensors (Li-190R quantum sensor, LI-COR Biosciences, USA) located in four different locations, totaling 16 sensors, (2) above canopy at 35 m height (PAR_{eco}) via single sensor (Li-190SZ quantum sensor, LI-COR Biosciences, USA).

One-sided LAI was calculated via concurring PAR measurements conducted below and above the canopy using inverted Beer–Lambert equation with direct beam and diffuse radiation separated. The extinction coefficient was determined from pine trees in the study site in 1998 (Mäkelä et al., 2006). Relative humidity and air temperature (T_a) were measured via Rotronic MP102H RH/T sensor at various heights (i.e., 0.4, 1.5, 3.3, 5.8, 8.8, 16.8, and 21.6, and 27 m). Soil temperature (T_s) was measured at 0.05 m depth via thermistors (KTY-81), while volumetric soil water content (SWC) at 0.1 m via (Delta-T ML2). Precipitation (P) was measured via weighing gauge (OTT Pluvio-2). Wind speed (u) was measured via Thies 2D ultrasonic anemometer at various heights (4.2, 8.4, and 16.8 m).

2.3. Process-model predictions

We used a process-based multi-layer ecosystem model pyAPES (Launiainen et al., 2015; Leppä et al., 2020) to simulate the effects of UR and MH, as well as the effect of IAVW. The model has been thoroughly tested at the site of this study and shown to well predict the above and sub-canopy carbon, water, and energy fluxes, canopy microclimate, and soil moisture and temperature profiles (Launiainen et al., 2015) and long-term trends in GPP and ET (Launiainen et al., 2022). Here, we will solely focus on modeled forest floor evaporation (Ef_{mod}), canopy evaporation (Ec_{mod}), tree transpiration (Tr_{mod}), ecosystem evapotranspiration (ET_{mod}), and ecosystem photosynthetic productivity (GPP_{mod}), where "mod" denotes the model-based fluxes.

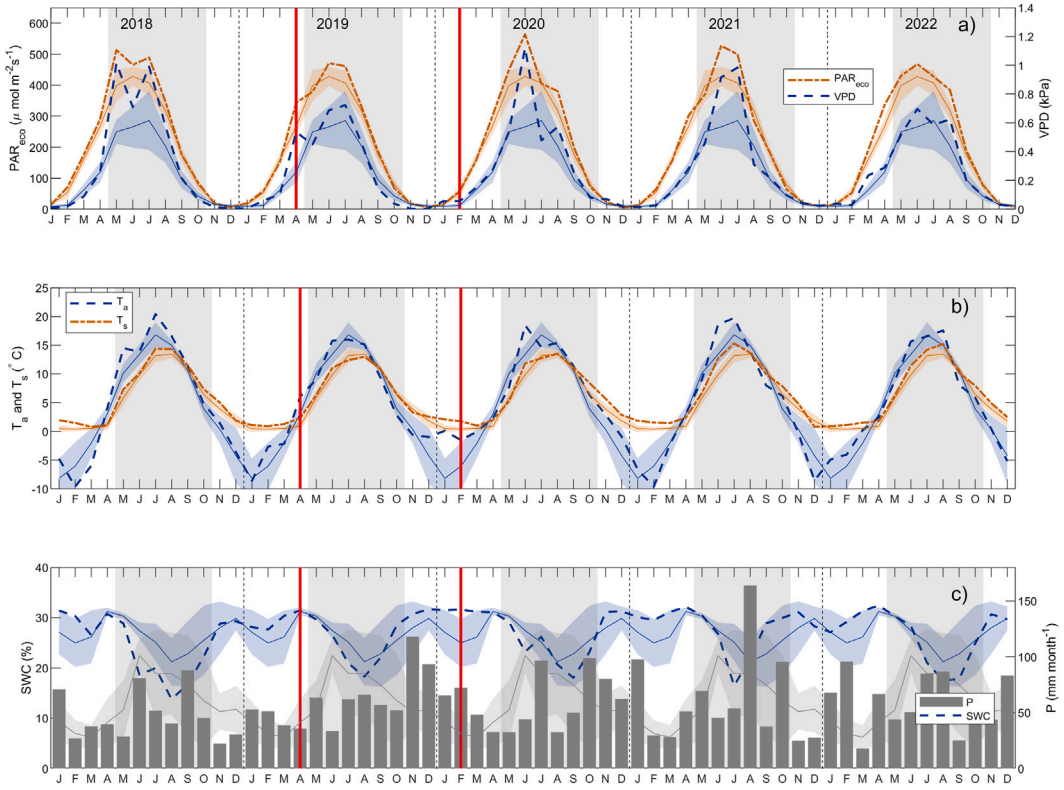

Fig. 3. Environmental conditions during the study years: (a) mean photosynthetic active radiation above the canopy (PAR_{eco}) (orange dash-dotted line) and monthly mean vapor pressure deficit (VPD) (blue dashed line) and, (b) monthly mean air (T_a) (blue dashed line) and soil temperature (T_s) (green dashed line), (c) monthly cumulative precipitation (P) (gray bar) and mean volumetric soil water content (SWC) (blue dashed line). The long-term averages (2009–2017, thin lines) and one standard deviation range (shaded) are given as references, and the respective variables are shown with their corresponding colors. The gray areas represent the growing season (May–Oct). The vertical red lines highlight the understorey removal (UR) and main harvest (MH), respectively.

To mimic the thinning, we consider the stand initially consists of six PlantTypes: overstorey pine, spruce and deciduous trees, understorey spruce, and deciduous species (DBH ≤ 7 cm), and forest-floor shrubs. We used measured species-specific DBH distribution (from 2019 and 2020) within the 200 m radii from the EC tower to estimate the vertical leaf-area density (*lad*) profiles and LAI of each PlantType. The needle/leaf masses for each DBH class and species were predicted by allometric equations (Repola, 2008, 2009), and converted to leaf area using the specific leaf area values from Härkönen et al. (2015). Finally, we applied a site-adapted relationship between DBH and tree height and distributed the leaf area vertically using crown biomass models (Tahvanainen and Forss, 2008). The obtained integrated *lad* distributions of overstorey (DBH > 7 cm) and understorey (DBH ≤ 7 cm) trees are shown in Fig. 4a.

Apart from the harvesting-induced changes in LAI and *lad* (Table 1), we use the model version and parameterization of Launiainen et al. (2022) for the study site. In UR in 2019, we assume understorey tree LAI was reduced by ca. 70% while the overstorey trees were left intact. In MH, the overstorey pine LAI was then further decreased by 40% and that of spruce and deciduous by 45%, while the gradual recovery from first to second post-thinning year (Section 2.1) was assumed uniform across all PlantTypes. In absence of data, forest floor shrub LAI was set constant at 0.5 m^2 m^{-2} in all scenarios.

To evaluate the management and IAWV effects, we simulated half-hourly carbon, water, and energy exchange using the measured above-canopy meteorological forcing from 2018–2021. In total, we ran 4 (LAI) ×4 (year) scenarios and evaluated the effect of IAWV as the variability among the cumulative growing season fluxes representing each year in a given LAI-scenario, while the thinning effects are computed as the mean difference between the pre-thinning and respective LAI-scenario averages. In discussion, we use pyAPES also to generalize the results over a larger LAI range and thinning intensities.

3. Results

3.1. Weather

Fig. 3 and Table 2 summarize monthly, growing season, and annual meteorological conditions during the study period (2018–2022), and compare them with the long-term (2009–2017) averages.

Due to the northern latitude, the seasonal cycle in solar radiation, air temperature, and air humidity are strong. The PAR_{eco} was similar to the long-term averages, except in June 2020 and June–July 2021 which were less cloudy than typical (Fig. 3a). There was considerable more variability in air temperature (Fig. 3b), the most notable being the warm winter (yet mostly below 0 °C) of 2019–2020. Growing season soil temperature was above the long-term averages by ca. 5%–10% in 2018–2022, except 2019 (Table 2).

The annual precipitation and mean annual soil moisture were similar to the long-term averages, except in the dry summer of 2018 (Fig. 3c), during which the large parts of Nordic forests were suffering from drought but the study site was not strongly affected (Lindroth et al., 2020). Monthly average soil water content varied between ca. 35% and 12% (Fig. 3c), being well above the wilting point (ca. 3%–5% Duursma et al., 2008).

Vapor pressure deficit (VPD) strongly varied over growing seasons, especially in June–August, typically peaking in late June (Fig. 3a). The atmospheric evaporative demand, calculated following Priestley and Taylor (1972) integrated over the growing seasons did not significantly vary across the study years, deviating only less than 4% compared to the mean growing season sum (674 mm).

Table 2
Annual and growing season mean of volumetric soil water content (SWC, %), soil temperature at 5 cm depth (T_s, °C), air temperature at 16.8 m (T_a, °C), global radiation (R_g, W m^{-2}), below and above canopy photosynthetic active radiation (PAR_{ff}, PAR_{eco}, μmol m^{-2} s^{-1}) and sum of precipitation (P, mm m^{-2}). The growing season values are shown inside parentheses.

Year	SWC	T_s	T_a	R_g	PAR_{ff}	PAR_{eco}	P
2018	25 (20)	6.4 (10.8)	5.3 (13.6)	114 (174)	31 (56)	221 (346)	562 (335)
2019	27 (24)	6 (10)	4.9 (11.3)	108 (162)	43 (67)	208 (316)	724 (334)
2020	27 (23)	6.5 (10.5)	6.4 (12.3)	114 (177)	78 (127)	219 (345)	715 (354)
2021	28 (26)	6.6 (11)	4.3 (12.6)	109 (167)	66 (111)	207 (321)	725 (466)
2022	27 (23)	6.5 (10.9)	5.1 (12)	115 (173)	60 (105)	217 (330)	734 (359)
2009–2017	27 (26)	5.6 (9.9)	4.4 (11.6)	95 (146)	39 (61)	193 (299)	706 (459)

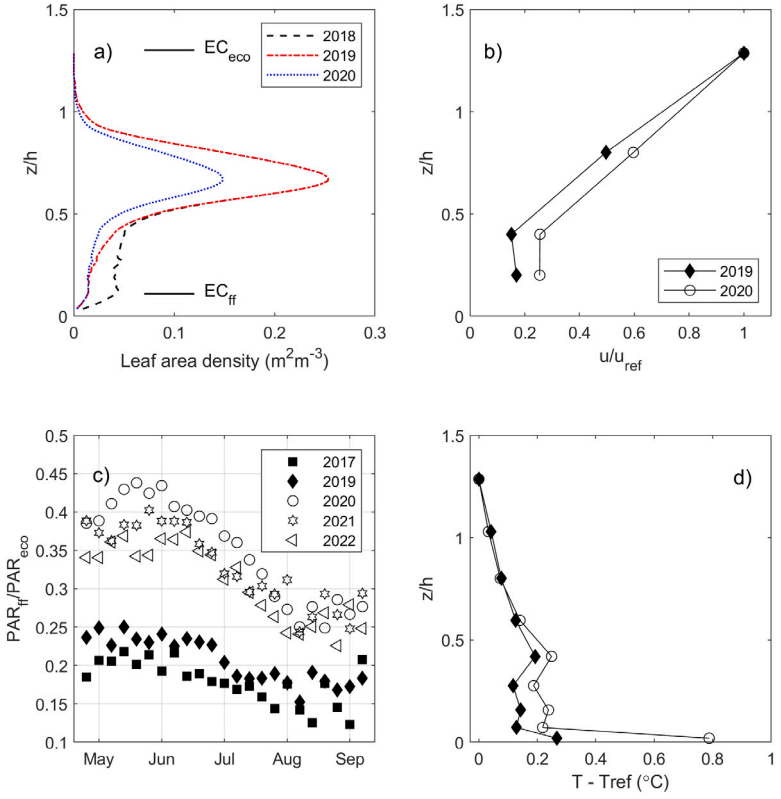

Fig. 4. Thinning induced changes in (a) leaf area density (*lad*) before (2018), after UR (2019), and after MH (2020). The z/h is height above the ground level relative to the mean canopy height; (b) the ratio of mean growing season wind speed measured at 4.2, 8.4, 16.8 m to that at 27 m (u_{ref}), (c) the weekly mean ratio of photosynthetic active radiation below (PAR_{ff}) to above-canopy (PAR_{eco}) during growing seasons, (d) the difference of mean growing season daytime air temperature (measured at 0.4, 1.5, 3.3, 5.8, 8.8, 16.8, and 21.6 m) from the value at 27 m (T_{ref}) in 2019 (after UR) and 2020 (after MH).

3.2. Thinning-induced changes in subcanopy microclimate

The UR was focused on trees with DBH < 7 cm, and thus reduced *lad* in the lower canopy only. The main harvest (MH) resulted in a near uniform *lad* reduction in the main canopy (Fig. 4a), with negligible changes in species composition (Fig. 1b). Following UR in 2019, light availability at the forest floor improved only marginally, while a major increase followed MH in 2020 (Fig. 4c). In the first (2021) and second (2022) post-thinning years, the growth of new foliage (Section 2.1) caused a slight reduction in the PAR_{ff}/PAR_{eco} ratio, especially visible in the summer months (Fig. 4c). Also mean wind speed inside and below the canopy relative to above-canopy increased after MH (Fig. 4b), indicative of weaker momentum absorption in the upper canopy. In Fig. 4b, only periods with near-neutral conditions (−0.05 < z/L < 0.05, where z is the measurement height) and northern wind direction were considered. The difference of daytime mean air temperature below the canopy and above the canopy slightly increased after MH (2020) compared to 2019 (Fig. 4d).

3.3. CO_2 fluxes

Due to the Northern location of the site, the seasonal cycle of CO_2 exchange is strong. Both ecosystem and forest floor photosynthesis and respiration were smallest in winter months (Dec–Feb), and peaked in the summer (June–Aug) (Fig. 5). Due to weak photosynthetic activity during winter months, the forest was a source of carbon (NEE > 0) typically from October to April. The forest became a CO_2 sink in April, reaching its maximum CO_2 uptake (NEE < 0) in July when also GPP_{eco} and R_{eco} were the highest. The year of MH (2020) was exempt from such behavior with a clearly shorter summer sink period (Apr–Aug) and noticeably lower monthly GPP_{eco}.

The forest floor was a consistent source of carbon (NFFE > 0, Fig. 6a) throughout the year, as the weak photosynthetic productivity (GPP_{ff}, Fig. 6b) was not sufficient to compensate for strong respiration (R_{ff}), which steadily constituted ca. half of the ecosystem respiration (Figs. 5 & 6c).

The annual NEE showed strong variability between −296 and +115 g C m^{-2} yr^{-1} over the five study years (Fig. 6a). Net annual

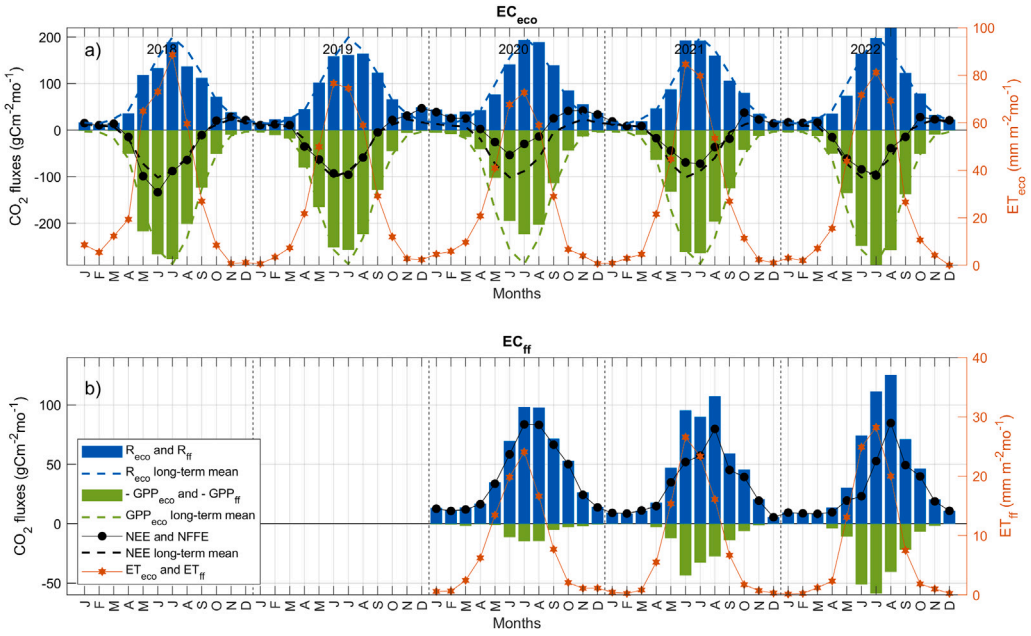

Fig. 5. Monthly sums of CO_2 and H_2O fluxes (a) at the ecosystem level (EC_{eco}), consisting of gross primary production (GPP_{eco}), respiration (R_{eco}), net ecosystem exchange (NEE), and evapotranspiration (ET_{eco}); (b) at the sub-canopy level (EC_{ff}), consisting of gross primary production of forest floor (GPP_{ff}), forest floor respiration (R_{ff}), net forest floor exchange (NFFE) and forest floor ET (ET_{ff}). For visual clarity, GPP_{eco} and GPP_{ff} are shown with negative sign. Long-term means (2009–2017) of NEE, GPP_{eco} and R_{eco} are shown with dashed lines in corresponding colors in panel (a).

CO_2 uptake was the highest in 2018 when the forest was intact, and decreased by ca. 25% in 2019 following UR. It further decreased after MH, turning the forest from a long-term sink into an annual CO_2 source (NEE +115 g C m^{-2} yr^{-1}) in 2020. However, the annual NEE partly recovered already in the first (2021) and second (2022) post-thinning years, yet the net annual uptake still remained below the long-term average (−271 ± 24 g C m^{-2} yr^{-1}, Launiainen et al. (2022)). Accordingly, the light response of NEE showed parallel changes throughout growing season and in between years (Fig. 7a), with the strong decrease in CO_2 uptake in 2020 after the MH being the most detectable change.

The annual GPP_{eco} was nearly similar in 2018 when the forest was intact and in 2019 following UR (1202 and 1189 g C m^{-2} yr^{-1}, respectively) (Fig. 6b). These values are typical to the pre-thinning average GPP_{eco}; 1212 ± 60 g C m^{-2} yr^{-1}, Launiainen et al. (2022). In 2020 following MH, GPP_{eco} decreased by ca. 20% to 967 g C m^{-2} yr^{-1}, and then gradually recovered to 1114 g C m^{-2} yr^{-1} in the first post-thinning year (2021) and to 1205 g C m^{-2} yr^{-1} in the second post-thinning year (2022). GPP_{ff} was considerably smaller than GPP_{eco} being only 5% of long-term averages in 2020, yet monotonously increasing to 12 and 16% in 2021 and 2022, respectively (Fig. 6b).

R_{eco} was slightly higher in 2019 (Fig. 6c) in comparison to both 2018 and long-term average (933 g C m^{-2} yr^{-1} Launiainen et al., 2022). It further increased by ca. 10% in 2020 (to 1082 g C m^{-2} yr^{-1}) following the MH, and equivalently retraced back in 2021 to the level of 2019. Later, it presented a slight increase (ca. 50 g C m^{-2} yr^{-1}) in 2022. R_{ff} steadily constituted approximately half of R_{eco} in both 2020 and post-thinning years.

The base respiration rates at the reference temperature of 10 °C (R_c) obtained for growing seasons are shown in Table C.6 (see Appendix C). For R_{ground}, R_c gradually decreased between 2018–2020, while for R_{ff}, it was similar in 2019 and 2020, then increased in 2021 and 2022. For R_{eco}, it varied within a small range without presenting any pattern.

3.4. H_2O exchange

The seasonal cycle of the ecosystem and forest floor ET resembles that of GPP, being negligibly low in winter and peaking in June–July (Fig. 5). Annual cumulative ET_{eco} was close to the long-term average (359 ± 19 mm H_2O m^{-2} yr^{-1} Launiainen et al., 2022) during all studied years (Fig. 6d). Monthly sums and annual cumulative forest floor water fluxes (ET_{ff}) typically constituted ca. 20% of long-term average of ecosystem ET in 2020–2022. Contrary to NEE, the relationship between ET_{eco} and incoming PAR_{eco} is near-linear (Fig. 7b), with the slope increasing from May to July–Aug, likely due to a combined response to enhanced needle- and ecosystem-level photosynthetic capacity and thus transpiration towards the summer (Fig. 7a, Kolari et al. (2014)) and increased atmospheric evaporative demand. There is a striking

Table 3
Growing season (May–October) and non-growing season (January–April + November–December) sums of R_{eco}, GPP_{eco} (g C m^{-2}) and ET_{eco} (mm H_2O). The values in parenthesis show the contribution to the annual sum (%). Ecosystem WUE (WUE_{eco}, µmol CO_2 m^{-2} s^{-1} per mmol H_2O m^{-2} s^{-1}) is reported only for the growing season.

Variable	Year	Growing season	Non-growing season
R_{eco}	2018	763 (84.2)	142 (15.8)
	2019	778 (79.7)	198 (20.3)
	2020	826 (76.4)	255 (23.6)
	2021	819 (84.5)	150 (15.5)
	2022	858 (84.3)	160 (15.7)
GPP_{eco}	2018	1136 (94.5)	66 (5.5)
	2019	1069 (90)	119 (10)
	2020	880 (91.1)	86 (8.9)
	2021	1021 (91.7)	92 (8.3)
	2022	1124 (93.3)	80 (6.7)
ET_{eco}	2018	321 (87.1)	47 (12.9)
	2019	301 (88.7)	38 (11.3)
	2020	276 (85.8)	45 (14.2)
	2021	301 (90)	33 (10)
	2022	303 (90.4)	32 (9.6)
WUE_{eco}	2018	6.6	–
	2019	6.9	–
	2020	5.7	–
	2021	6.8	–
	2022	6.7	–

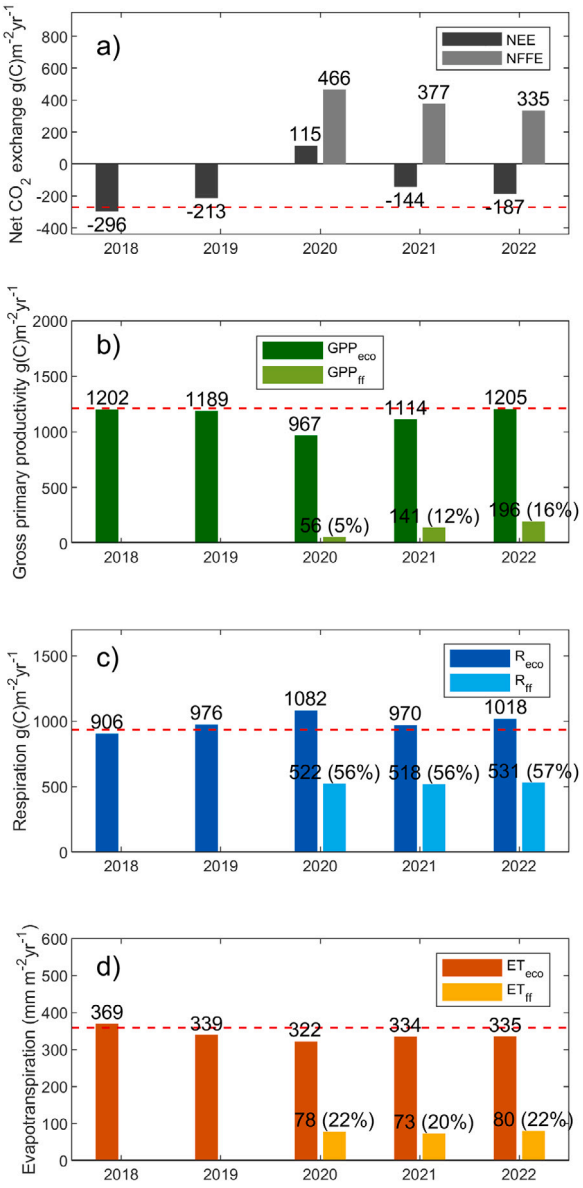

Fig. 6. Annual CO_2 and H_2O fluxes: (a) net ecosystem exchange (NEE) and net forest floor exchange (NFFE), (b) ecosystem (GPP_{eco}) and forest floor (GPP_{ff}) gross-primary productivity, (c) ecosystem (R_{eco}) and forest floor (R_{ff}) respiration, (d) ecosystem (ET_{eco}) and forest floor evapotranspiration (ET_{ff}). Percentages shown in parenthesis represent the proportion of the forest floor to the long-term (2009–2017) means of ecosystem-level fluxes depicted by horizontal dashed red lines (Launiainen et al., 2022).

dissimilarity between NEE and ET_{eco} response to thinning: the latter showed only a minor reduction following the MH (in May–July 2020, Fig. 7b).

Stand transpiration was the main component of ET_{eco}, contributing up to 90% of dry-canopy (i.e. in absence of recently intercepted precipitation evaporating from the canopy) ET in late growing season and autumn 2019 (Fig. 8). The contribution clearly decreased after MH (2020, 70%, with a slight recovery in 2022 (75%). The relationship between T_{stand} and ET_{eco} was near-linear in all study years.

Ecosystem water use efficiency (WUE_{eco}) was 6.6 and 6.9 μmol CO_2 m^{-2} s^{-1} per mmol H_2O m^{-2} s^{-1} in 2018 and 2019 (after UR), resembling the long-term averages in Launiainen et al. (2022) (Table 3). After MH, it dropped to 5.7 in 2020 but recovered to 6.8 & 6.7 in 2021, and 2022 respectively.

4. Discussion

4.1. Effect of inter-annual weather variability

Weather conditions were rather similar in all years except for dry summers of 2018 and 2022 (Fig. 3c), and the warmer than average winter of 2019–2020 (Fig. 3b). However, the growing season and annual sums of NEE and ET_{eco} in 2018 were similar to long-term averages, indicating a negligible effect of the drier summer, as already reported in another study by Lindroth et al. (2020).

The warmer winter 2019–2020 resulted in no significant changes in GPP and ET (Fig. 5). It however likely affected the respiration, increasing the annual R_{eco} of both 2019 and 2020 by ca. 20 and 50 gC, respectively (Fig. 5a), when comparing Dec–Jan–Feb cumulative fluxes with long-term averages (Launiainen et al., 2022). At large, there was a steady contribution of growing season sums into annual sums,

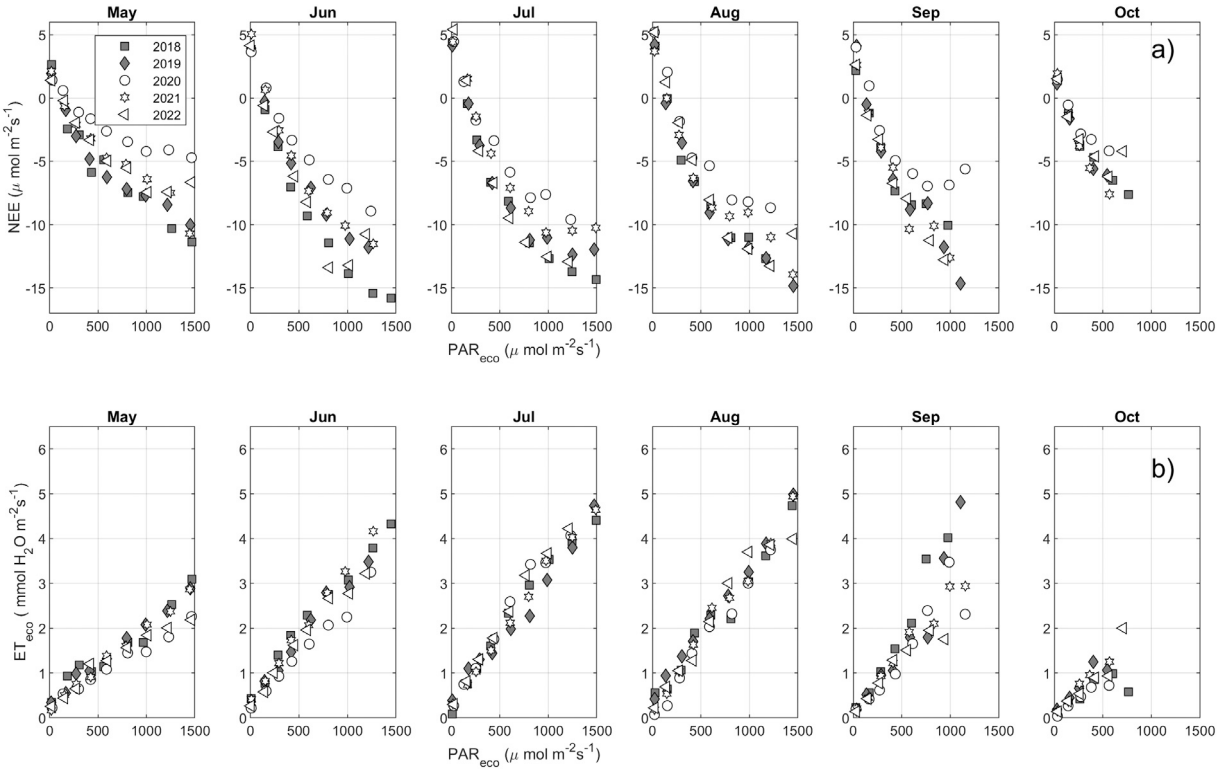

Fig. 7. Response of (a) net ecosystem CO_2 exchange (NEE) and (b) ecosystem evapotranspiration (ET_{eco}) to photosynthetic active radiation above the canopy (PAR_{eco}) for each growing season month in 2018–2022. PAR_{eco}, ET_{eco}, and NEE are screened for environmental extremes as described in Appendix A.

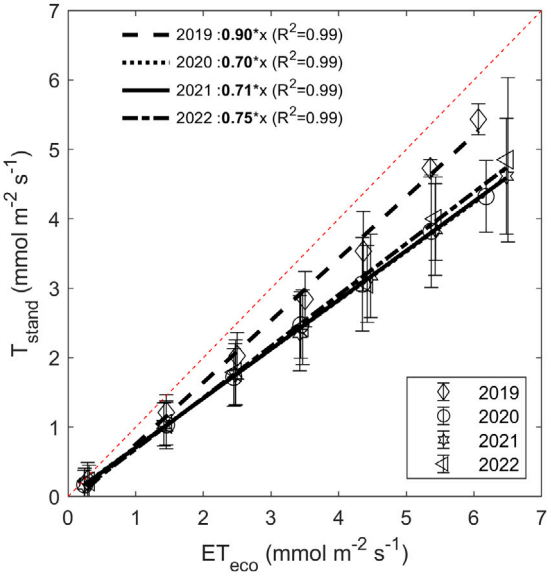

Fig. 8. Relationship of estimated stand transpiration (T_{stand}, see Section 2.2.2) and measured dry-canopy ET_{eco} for each year with coinciding below- and above-canopy EC measurements, i.e., 2019 (Aug-Dec), 2020, 2021, and 2022. Means of binned half-hourly values are shown with error bars of one standard deviation. Lines represent linear least-square regressions to the corresponding year's means. The diagonal dashed-red line is the 1:1 line.

i.e. 90% for GPP_{eco}, 75% for R_{eco}, and 85% for ET_{eco} (Table 3). Minor contribution of non-growing season sums indicates the negligible role of winter-time fluxes, especially for ET and GPP.

To further investigate the impact of IAWV on annual GPP_{eco} and R_{eco}, we reconstructed the cumulative fluxes for 2019 and 2020 using the corresponding weather data in Eqs. (C.2) & (C.1) and fixing the gap-filling parameters to their mean seasonal cycles from 2009–2017 period (Section 2.2.5). The results of GPP_{eco} (Fig. 9b) shows that the reconstructed fluxes fall within the inter-annual flux variability range (standard deviation 4%, when fluxes are normalized with the mean of long-term fluxes), indicating the IAWV cannot explain the found differences in GPP_{eco} as this variability is clearly smaller than the observed changes after thinning. Similar conclusion can be drawn for the results of R_{eco} of 2019 (Fig. 9a), whereas the reconstructed fluxes of

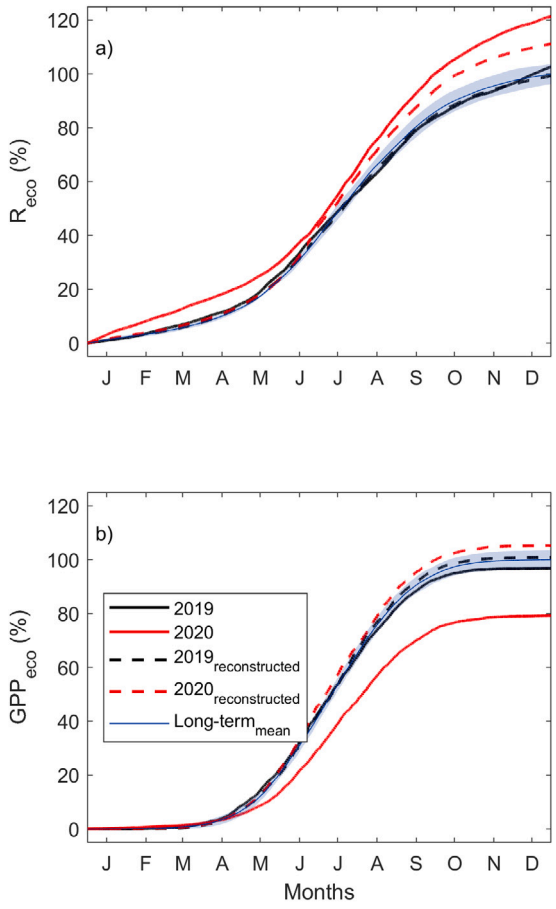

Fig. 9. Annual cumulative (a) ecosystem respiration (R_{eco}), and (b) gross primary production (GPP_{eco}) reconstructed via gapfilling parameters of 2019 (black line) and 2020 (red line), and via long-term averages (2019LT and 2020LT) shown with dashed lines with corresponding colors of the year. The mean of long-term constructed fluxes (LT_{mean}) is shown with thin-blue line and a standard deviation with light-blue shaded area. All values shown are normalized with the LT_{mean} annual sum.

R_{eco} of 2020 slightly exceed (ca. 5%) the inter-annual range, indicating the effect of a minor role of IAWV, especially the warm winter. It is worth noting that this simple modeling is based on only a few driving variables, i.e., temperature for respiration and, temperature and PAR for gross-primary productivity. This makes it potentially prone to at least temporal biases in case the seasonal pattern of driving variables differs significantly from 2009–2017 period used to derive the average seasonal cycle of light-response and respiration parameters (Eqs. (C.2) & (C.1); Appendix C).

The small role of IAWV on gross-primary productivity and evapotranspiration is further supported by the process-model simulations. Fig. 10 shows the growing season (May–Oct) ET components and GPP_{eco} for each forest stage (intact in 2018, 2019 after UR, and 2020 after MH, 2021 as 1st PT) under weather forcings from four different years. The simulations revealed markedly higher weather sensitivity (effect of IAWV) in water fluxes than to photosynthetic productivity. Despite similar evaporative demand across the years (Section 3.1), precipitation and VPD patterns were different during the summer months (Fig. 3a). The effect of such variation is clearly more pronounced on evaporative water losses from canopy intercepted water and forest floor rather than on photosynthetic production or transpiration rate. This is primarily due to the stomatal control aiming to maximize photosynthetic carbon gain while minimizing transpirative water losses (Katul et al., 2010; Medlyn et al., 2012).

4.2. Effect of thinning on carbon and water fluxes

Based on the previous section, we conclude the growing season or annual CO_2 fluxes and ET were not significantly affected by IAWV. Also, the uncertainty of annual NEE, GPP_{eco} and R_{eco} stemming from gap-filling and flux partitioning (Appendix C) is small compared to the observed changes in fluxes. Thus, in the next sections we interpret the observed changes (or their lack of) solely as thinning responses.

To put our results in the context of earlier findings, we summarized the literature reported (hemi) boreal and temperate forest thinning effects in Table 4. The changes shown represent the immediate responses (i.e., the first post-thinning year) with respect to either single pre-thinning year or long-term averages of annual fluxes. The comparison is done assuming the IAWV has no significant impact, and discards the uncertainty stemming from different types of analysis among the reviewed studies.

4.2.1. Understorey removal

Following UR in 2019, net carbon uptake decreased by ca. 20%. In UR, the suppressed small-diameter trees were felled, which resulted in ca. 10% leaf area loss (Table 1). However, this had a very minor effect on annual GPP_{eco} (Fig. 6b) as the removed foliage was mainly light-limited (Fig. 4a) due to the closed canopy (high pre-thinning LAI) (Section 2.1). Since the light condition at the forest floor enhanced only marginally (Fig. 4c), we believe UR did not markedly affect GPP_{ff}. The process-model simulations support this interpretation, and suggest the LAI reduction in UR would reduce growing-season GPP_{eco} only ca. 3%–4% (or ca. 40 g C m^{-2} yr^{-1}) (Fig. 10). Due to IAVW and uncertainties associated with micrometeorological flux measurements and partitioning, such a small change can well remain unnoticeable in the EC data.

Contrary to the unchanged GPP_{eco}, the annual R_{eco} increased by ca. 8% (or 70 g C m^{-2} yr^{-1}) compared to 2018 (Fig. 6, Table 3). As shown in Table 1, the UR provided additional input of ca. 45 g C m^{-2} fine cutting residues and ca. 515 g C m^{-2} coarse woody debris (CWD; including trunks, branches and coarse roots) (Aalto et al., 2023). The ratio of decomposed biomass to the initial litter biomass as a function of time is often approximated via exponential function $M(t)/M_0 = exp(-k\,t)$, where the single parameter k is the decomposition rate (Olson, 1963). For coniferous foliage and fine-root litter, k varies between 0.15 and 0.4 yr^{-1} (Song et al., 2021; Johansson et al., 1995; Prescott et al., 2000), while k between 0.03 and 0.06 yr^{-1} is typical for CWD in similar climate (Zell et al., 2009; Tarasov and Birdsey, 2001). During the first year after UR, this would correspond to additional heterotrophic respiration around 6–15 and 16–30 g C m^{-2} yr^{-1} from fine-cutting residue and CWD, respectively. This additional input together with the slightly increased respiration in Dec 2019 due to warmer weather (Appendix A) likely explains the increased R_{eco} in 2019 compared against typical annual levels observed at the site. It is important to note that fine-root litter decomposition is not included in fine-cutting residue calculations due to lacking estimations. In addition, there was snow damages in winter 2019, affecting ca. 35 trees per hectare in varying DBH. This may have also possibly increased R_h.

The growing season and annual ET_{eco} showed no significant response to UR, and were only slightly below the long-term averages in 2019 (Fig. 6d and Table 3). Neither did the radiation response of ET_{eco} change (Fig. 7b), and T_{stand} (estimated via EPL20) comprised as high as 90% of ET_{eco} (Fig. 8). For coniferous boreal forests, this ratio is in the upper range reported (see e.g. Kozii et al., 2020), suggesting dry-canopy ET of closed-canopied forest was mainly from transpiration during the latter part of the growing season. The minor impact of UR on ET_{eco} is supported by the model predictions (Fig. 10c), showing only a marginal reduction compared to the intact forest in 2018. The lack of change in ET was likely due to the increase in Ef_{mod}, compensating for the reduced Tr_{mod} after UR (Fig. 10a and b).

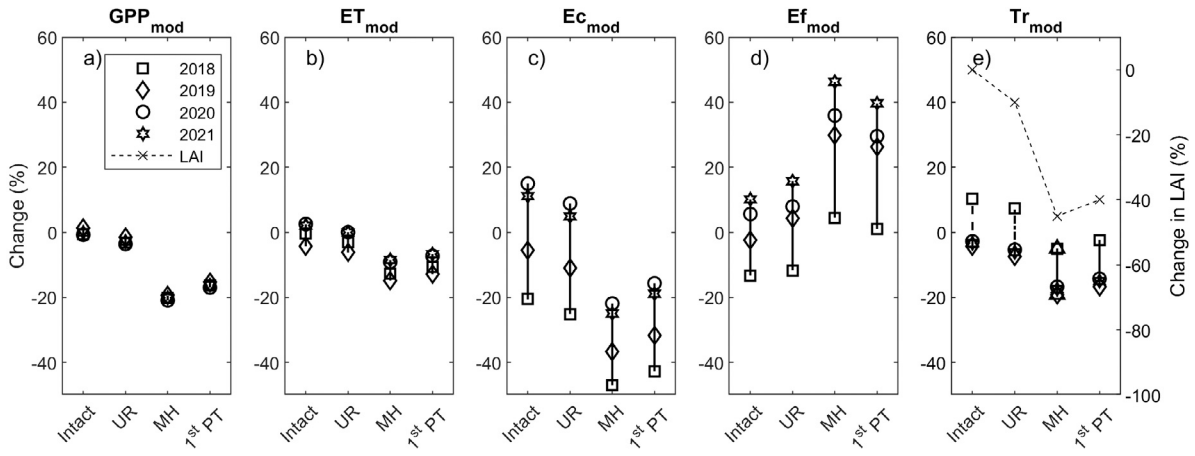

Fig. 10. Thinning response of ecosystem GPP and water flux components estimated via pyAPES model (Section 2.3). The numbers in *y*-axis show the relative change compared to the intact-forest. This reference flux is defined as the mean of growing season fluxes estimated by running the model with weather forcing data from all the study years. Consequently, the variability within a given forest stage (i.e. intact, UR, MH, 1st PT) depicts the effect of inter-annual weather variability, while the mean difference between forest stages represents the thinning impact (or recovery). Dashed line in panel (e) shows the LAI relative to the intact forest (in 2018).

Table 4
Summary of studies investigating the effect of thinning on ecosystem level water and carbon fluxes, showing site characteristics, basal area (BA - m^2 ha^{-1}) before harvesting with thinning intensity (%) shown in the bracket, one-sided leaf index (LAI - m^2 m^{-2}) with foliage loss (%) in the bracket, the immediate change (i.e., first post-thinning year) in GPP_{eco}, R_{eco}, NEE, T_{stand}, ET_{eco} and WUE_{eco} with respect to the pre-harvesting year or long-term average (the signs "↑, ↓, and ⇔" indicate an increase, a decrease, and no significant change, respectively). Negative NEE (R_{eco} - GPP_{eco}) represents a sink of CO_2, hence "↑" sign indicates diminishing net carbon sink strength. The dominant tree species are Scots pine (SP), White pine (WP), Loblolly pine (LP), Norway spruce (NS), Sitka spruce (SS), Oak (O), mixed (M), European beech (EB), Birch (B). The studies are first segregated based on the regions, then sorted with ascending harvesting intensity (BA removal) within each.

Region	Study	Location	Forest type (age)	BA	LAI	GPP_{eco}	R_{eco}	NEE	T_{stand} (ET_{eco})	WUE_{eco}
	Skubel et al. (2017)	Canada (ON)	WP (74)	36 (13)	4.3 (38)				↓ (↑)	
	Lindroth et al. (2018)	Sweden	SP (100)	46.7 (21)	4-5 (38-50)	↓	↓	↑		
	Lagergren et al. (2008)	Sweden	SP (50)	29.1 (24)	4.6 (25)				↓ (⇔)	
(Hemi)	Aun et al. (2021)	Estonia	SP (45)	31.8 (24)				↑		
Boreal	Vesala et al. (2005)	Finland	SP (40)	24.3 (26)	4 (25)	↓	↓	⇔	↓(⇔)	
	Aun et al. (2021)	Estonia	SP (25)	27.2 (31)				↑		
	This study	Finland	SP (58)	31 (40)	4 (45)	↓	↑	↑	↓ (⇔)	↓
	Leppä et al. (2020)	Finland	SP	36 (70)	(52)				(↓)	
	Korkiakoski et al. (2023)	Finland	SP	36 (70)	(52)	↓	↓	↑		
	Saunders et al. (2012)	Ireland	SS (20)	43.9 (11)	2.6 (13)	↓	↓	↑		
	Saunders et al. (2012)	Ireland	SS (18)	48.2 (17)	3 (18)	↑	⇔	↓		
	Granier et al. (2008)	France	EB (32)	24 (24)	3.7 (35)	↑	↑	↓	(↑)	
Temperate	Granier et al. (2008)	France	EB (38)	26 (25)	3 (33)	↓	↓	↑	(↓)	
	Misson et al. (2005)	US (CA)	PP (10)	6.3 (31)	1.4 (34)	↓	⇔	↑		⇔
	Dore et al. (2010)	US (AZ)	PP	20 (35)	1.5 (40)	↓	↓	↑	(↓)	⇔
	Wilkinson et al. (2016)	UK	O (70s)	25 (36)		⇔	⇔	⇔		

4.2.2. Main harvest

Contrary to our hypothesis (H3), the forest became an annual carbon source following MH in 2020 (Fig. 6a). This was a result of increased respiration and strongly decreased photosynthetic CO_2 uptake (Fig. 6b and c). The reduction of GPP_{eco} in 2020 compared to the preceding year was ca. 20%, which is significantly lower than the foliage loss, i.e., 40%–45% (Table 1). The post-thinning decrease of GPP is a uniform finding across the reviewed studies in the boreal region (Table 4). In our case, the strength of observed thinning response was well in line with the process-model predictions (Figs. 10 & 11). The light interception by trees and hence light use efficiency (LUE) is a non-linear function of LAI (Mäkelä et al., 2008). Thus the leaf-level LUE increased after thinning due to more even distribution of radiation throughout the tree canopy, enabling the previously shaded leaves in lower canopy to photosynthesize more than before thinning (Wilkinson et al., 2016). This increase of needle-level photosynthesis primarily explains the moderate reduction in GPP_{eco} and transpiration compared to foliage loss as hypothesized (H1 and H4). We note that also improved water and nutrient availability and changes in canopy temperature and humidity profiles may also catalyze the enhanced needle and tree-level CO_2 uptake after thinning. These feedbacks were, however, not addressed here.

Annual GPP_{ff} in 2020 after MH was only 5% of the long-term average of GPP_{eco}. This contradicts the narrative that thriving ground vegetation plays an important role in the weak response of NEE (and its immediate recovery) to thinning (Vesala et al., 2005; Wilkinson et al., 2016, see summary of thinning studies in Table 4). The low photosynthetic activity at forest floor in 2020 might be due to the disturbance of ground vegetation, and the additional shading by the cutting residues left on the site (both in UR and MH). Another reason might be the post-thinning stress (Lagergren et al., 2008), indicating a slow acclimation of shade-adopted vegetation to drastically increasing light availability. In our case, we observed as much as a 90% increase in light availability at the forest floor (Fig. 4c). This is much greater than the 63% increase reported by Teramoto et al. (2019), while Son et al. (2004) reported 59% for similar BA removal ca. 40% in temperate forests. By the data available, we however cannot quantify the extent of how these potential reasons may explain the small contribution of GPP_{ff} to GPP_{eco} after thinning.

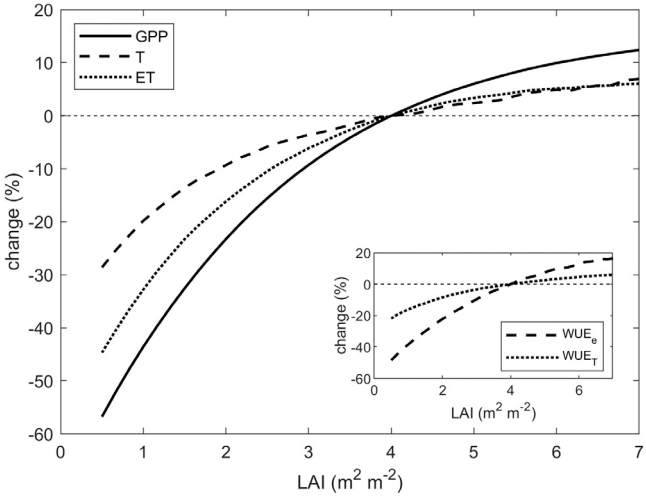

Fig. 11. Process-model predictions of the response of gross photosynthetic productivity (GPP), transpiration (T), and evapotranspiration (ET) as well as ecosystem water use efficiency (WUE_e) and stand transpiration use efficiency (WUE_T) for various thinning intensities. The figure shows the relative difference of each response variable with respect to the reference LAI = 4.0 m^2 m^{-2}.

The observed increase in R_{eco} was unexpected (contrary to H2). In fact, all previous studies in boreal forests reviewed in Table 4 have reported R_{eco} decrease after thinning, while the response has been less consistent for temperate stands (Table 4). In our study R_{eco} after MH was ca. 15% higher than the long-term averages, and our interpretation is the majority of the increase is related to the MH and a smaller fraction to the warm winter (Fig. 5a, Section 4.1). The fine-cutting residue and CWD left at the site in MH were ca. 80 and 870 g C m^{-2}, respectively. Using a similar estimate of litter turnover for UR, this would contribute approx. 58–115 g C m^{-2} yr^{-1} increase in heterotrophic respiration (including also the decomposition of UR-based cutting residue). This increase is likely partly compensated by reduced autotrophic respiration as a response to harvest and subsequently decreased photosynthetic productivity (R_a typically 40%–60% of GPP_{eco}; Ilvesniemi et al. (2009)).

The base ecosystem respiration at 10 °C (R_c, Table C.6) changes after thinning were in line with the changes in annual R_{eco}. On the contrary the R_c of forest floor respiration gradually increased even though annual R_{ff} remained similar across the years. The automatic chambers used to measure ground respiration (R_{ground}) contained no cutting residue, and the ground vegetation confined by the collar was not altered during the harvesting procedure. After harvests, the gradual reduction in base rate of R_{ground} is thus likely due to the loss of living root biomass (decreased R_a), which was partly compensated by the decomposition of fine roots of harvested trees (increasing R_h) as well as the increased autotrophic respiration of remaining trees. Despite our effort to interpret the respiration changes after thinning via possible mechanisms, it is painfully clear that quantitative understanding of ecosystem respiration and its partitioning after forest management operations requires further empirical and theoretical research.

Similar to UR, neither growing-season nor annual ET_{eco} did not markedly change after MH (Fig. 6d) and were only slightly below the long-term averages (contrary to H5). This led to a decrease in ecosystem water use efficiency (WUE_{eco}, Table 3), again as predicted by the biophysical theory (Fig. 11). The radiation response of ET_{eco} showed no significant differences (Fig. 7b) between the years. Noting the negligible effect of IAWV (see Section 4.1), the insensitivity of ET_{eco} to thinning in comparison to T_{stand} can only mainly be explained by the MH-induced redistribution of ecosystem water sources and thus components of ET_{eco}. The decrease in T_{stand} was smaller than the reduction in leaf area, as the increasing photosynthetic activity of the remaining trees led to increasing transpiration per unit leaf area (Figs. 10c, 11). Similar behavior in T_{stand} after thinning has also been reported earlier (Lagergren et al., 2008; Skubel et al., 2017; Leppä et al., 2020).

The model simulations suggest canopy interception evaporation (Ec_{mod}) decreased after thinning. This is in line with the observations of Balandier et al. (2022), showing the contribution of stand interception to ET_{eco} decreases as LAI decreases. Also Sun et al. (2017) reported reduced interception following a heavy thinning (ca. 50% BA removal). The increasing throughfall reaching the forest floor and increasing energy (light) availability and ventilation (Fig. 4c, b) then likely led to increased (1) transpiration from the ground vegetation, (2) evaporation from plant surfaces and soil at the forest floor. The latter is also partly affected by increased live or dead plant surface area at the forest floor, and more turbulent conditions and increasing wind speed in the trunk space (Fig. 4b), both of which accelerate evaporation from wet surfaces. Accordingly, both our observations (Fig. 8) and model simulations (Fig. 10) suggest that evaporation from the forest floor (E_{ff}) indeed increased after thinning, and further compensated the reduced T_{stand} (see also Kozii et al., 2020).

Growing season soil temperature was ca. 5%–10% above the long-term averages in 2020–2022 (Table 2). This slight increase, despite greatly increased light availability, suggests the excess energy at the forest floor (Fig. 4c) was mainly used for increased sensible and latent heat exchange. A similar conclusion was drawn by Lagergren et al. (2008) who observed no change in soil temperature (at 10 cm depth) after light thinning in a Scots pine-dominated hemi-boreal forest.

4.2.3. Post-thinning recovery and cumulative effects

The studied forest became a weak carbon sink already in the first post-thinning year (2021); this marks the second post-thinning growing season (see Section 2.1 for definitions). The sink further recovered in 2022, however, net carbon uptake still remained significantly below the long-term average (Fig. 6a). This is mainly due to R_{eco} staying ca. 10% above the long-term average (Fig. 6c). There was a large increase in GPP_{eco} already in the first post-thinning year, and the long term-average level was reached in the second post-thinning year in 2022 (Fig. 6b), despite LAI remaining significantly below the pre-thinning value (Fig. 10e).

Also GPP_{ff} gradually increased, its contribution exceeding 10% and further 15% of the long-term average of GPP_{eco} in the first and second post-thinning year, respectively (Fig. 6b). This is likely related to both increasing foliage at forest floor and acclimation to the increased light availability. A similar forest floor GPP (131 g m^{-2} yr^{-1}) as observed in 2021 in our study (Fig. 6b) was found by Kolari et al. (2006), who upscaled the chamber measurements in the same study site in

the second year after the first commercial thinning (Vesala et al., 2005). The gradual increase of GPP_{ff} highlights that the forest floor is more likely to play an important role in recovery rather than in the immediate response of NEE (or its lack of) to thinning (Vesala et al., 2005; Wilkinson et al., 2016).

The measured ET_{eco} remained slightly below the long-term averages both in 2021 and 2022. T_{stand} slightly increased and contributed 71 and 75% of ET_{eco} in 2021 and 2022, respectively (Fig. 8). Likewise, Ec_{mod} marginally increased, near-proportionally to the increased foliage (Table 1). The gradual change in GPP_{ff} is suggestive of a similar increase in forest floor transpiration. With that, in addition to the observed changes in T_{stand} and model results for Ec_{mod}, forest floor evaporation likely decreased in 2022 when compared to 2021, in accordance with model results for Ef_{mod}.

Compared to the long-term pre-thinning averages, the loss in cumulative ecosystem carbon sink between 2019 and 2022 was ca. 660 g C m^{-2}. In total, thinning (UR+MH) resulted in ca. 1500 gC m^{-2} of cutting residue left to the site (Table 1), which ultimately decompose increasing the heterotrophic respiration and decreasing the net ecosystem CO_2 sink. Noting that part of the cutting residues have already decomposed and included in 2019–2022 NEE sums (Sections 4.2.1 and 4.2.2), thinning can be estimated to yield roughly an additional *on-site* CO_2 source of ca. 1200 gC m^{-2} to be compensated for in the future. Assuming the forest CO_2 sink strength is similar to the long-term averages (−272 gC m^{-2} yr^{-1}) already in the third post-thinning year (2023), the compensation for such carbon sink loss would take roughly 8 years. This *payback-time* contradicts the narrative claiming the neutral *on-site* effect of thinning on carbon balance (Vesala et al., 2005; Lindroth et al., 2018). In this regard, harvesting the cut understorey trees as well as upper non-valuable crowns (coarse residues) might be considered positive for *on-site* carbon balance and to reduce the *payback-time* (Grelle et al., 2023).

It is important to note the envelope calculation above neglects the fact that there would be a natural self-thinning as the canopy reaches the upper limit of development, which would eventually reduce GPP_{eco}. Further, it is assumed that the forest's sink strength would ultimately reach to the long-term averages. This might not hold as NEE is the small difference between R_{eco} and GPP_{eco}, and any changes in the component fluxes with stand age and recovery from thinning may have major effect on NEE. Therefore, long-term monitoring of thinning recovery is necessary to quantify the cumulative effects of thinning on *on-site* carbon budget, and to benchmark ecosystem and forest models against directly measured flux data.

The climate impacts of thinning cannot, however, be evaluated solely based on *on-site* impacts on carbon balance and surface energy balance (i.e. albedo). Following thinning, 114 m^3 ha^{-1} of commercially valuable timber was extracted and transported from the site. This is equivalent of 2.4 kg C m^{-2} reduction in stand carbon stock, and the climate impact of such re-location of carbon storage depends heavily on harvested timber assortments and the ultimate use of wood products. In Finland, approximately 50%–60% of timber harvested from second commercial thinning of Scots pine dominated stands (as here) is small-diameter fibrewood (Niemistö et al., 2018). Thus, major part of the harvested timber from thinning is used for short-term products (i.e. paper, cardboard, bioenergy) and the associated carbon storage consequently emitted to the atmosphere within 2–4 years (turnover time ca. 0.3 y^{-1}; Pukkala (2014)). Thinnings are, however, necessary to allocate growth resources to fewer trees to produce good-quality large diameter timber for more long-term products (life time tens of years) at the end of rotation. It is thus imperative that the system boundaries (i.e. ecosystem or biome, including or excluding wood use) and timescales are well defined when climate effects of forest management operations or management chains are analyzed and communicated (Keenan, 2015; Soimakallio et al., 2016).

4.3. Role of thinning intensity

The model simulations (Fig. 11) suggest that thinning intensity (i.e. strength of BA or LAI reduction) and the initial canopy structure (i.e. LAI, lad, and species composition) jointly determine the magnitude of thinning response. In Fig. 11, the changes are shown in percentages with respect to the fluxes when one-sided LAI = 4.0 m^2 m^{-2}, which can be considered the upper limit for pine-dominated stands prior to thinning. Here, TR of one (i.e., uniform DBH removal) is considered. The model predictions suggest that for a given absolute change in LAI, the thinning responses became weaker the denser the forest is initially.

Our results showed that a moderate 10% reduction of initial LAI by UR did not change photosynthetic production and water fluxes, while a slight increase in respiration was found. This was likely because the fully developed overstorey canopy crown was not affected (see Section 2.1, Fig. 4a). Thus, the initial structure of the canopy crown or lad at large is also very important along with the thinning intensity because the change in those would primarily define the changes in the microclimate of trunk space and the forest floor. Accordingly, for the forests with small BA, i.e., not fully developed canopy crown, the change in canopy crown would not be as important.

One way to monitor the change in the canopy structure following thinning is to consider change in lad, which was shown only in one thinning-related study so far (Leppä et al., 2020). Another way is the thinning ratio (Section 2.1). In the case of spatially homogeneous stand structure and thinning, TR is a rather informative metric. TR of one indicates an equal removal of all DBH size-classes (uniform thinning), while smaller values can describe "low" thinning and higher values can describe "crown" thinning. In our study, TR of UR was 0.04, while TR of MH was 0.61, both classified as low thinning. Saunders et al. (2012) investigated a Sitka spruce-dominated temperate forest thinned in two consecutive years. In the first thinning, they applied a near-uniform thinning (TR 0.85), while the latter was thinning from above removing the dominant trees (TR 1.37). Wilkinson et al. (2016) investigated the effect of thinning in an Oak dominated temperate forest where so-called "intermediate" of low- and crown thinning is typically applied to the middle-aged forest. Vesala et al. (2005) applied a low thinning in the study site, while the thinning examined by Lindroth et al. (2018) was strictly done from below, where the TR of the dominant Scots pine was 0.81, and spruce was 0.55. Despite the strong variability in thinning intensity, TR, and forest attributes (e.g., age, LAI), there is a consistent reduction in photosynthetic productivity and respiration (except in the present study), a decrease of annual NEE in the coniferous forest studied (Table 4). Likewise, a consistent pattern showing reduced stand transpiration exists, while the ET was found conservative (no change) in the majority of the reviewed studies.

For temperate regions, however, the thinning responses are much less consistent (Table 4). This might be due to: (1) greater role of varying weather conditions, hence the growing season commencement and length, (2) varying resource availability (especially water and nitrogen), (3) greater overall variability in annual fluxes (Wilkinson et al., 2016), (4) more diverse species composition and management practices.

4.4. Critical remarks and future outlook

In the previous sections, we attempted to put our findings in the context of earlier studies and discuss the role of thinning intensity. This was however challenging due to various differences and uncertainties regarding study designs, measurements, data processing, and the application of thinning.

Given the size and variability of the source/sink area (i.e., footprint) seen by an eddy-covariance setup, the design of a thinning experiment is challenging. Thinning a particular sector around the EC tower is a common approach (Wilkinson et al., 2016), where data from the unthinned sector are used as a control. This is however constrained due

to possible heterogeneity of the forest existing prior to the thinning, different weather characteristics as well as limited data availability from each sector. An alternative approach is to thin the entire forest stand, and analyze the thinning effect by comparing pre- and post-thinning EC data (Vesala et al., 2005, this study). However, this approach is prone to the uncertainty related to inter-annual weather variability, which makes it difficult to separate management and weather-related effects on carbon and water fluxes (Aubinet et al., 2018; Foken et al., 2021). We tackled this issue using both a statistical approach (Fig. 9) and a process-based model (Fig. 10) predictions, and propose this approach should become more widespread in the future studies.

The models estimating the source area of EC fluxes assume homogeneous and flat terrain, which is often not the case in real landscapes. Furthermore, the surface roughness parameters (roughness length and displacement height) are demanding to estimate (see Appendix B), and their dependency on stand density and *lad* affected by thinning increase the potential uncertainties. Furthermore, many of the source area models are not strictly valid in the roughness sublayer (i.e. air layer extending approximately 2 to 5 times the canopy height above the surface). In some thinning studies (Dore et al., 2010), the fluxes exceeding the boundaries of the harvested area were discarded from the data set, while in many (Wilkinson et al., 2016; Lindroth et al., 2018, this study) it is assumed that the whole source area was within the harvested area. Our footprint analysis showed that daytime fluxes originated from the thinned area, whereas in nighttime some portion of the fluxes may include contributions from the un-thinned area (Fig. 1a). That said, to make sure the fluxes originate solely from thinned area, a suitable spatial extent of harvests should be ensured in the future studies.

Forests are multi-layer complex ecosystems. Due to contrasting responses of the respiration, photosynthesis, and evapotranspiration components at different compartments of the forest, the fluxes measured solely by above-canopy eddy covariance setup are not sufficient. Our results emphasize that additional monitoring of forest floor fluxes are highly beneficial and necessary to interpret the causal mechanisms and compensatory effects underlying the changes in ecosystem level carbon and water fluxes. To do so, laborious manual chamber measurements are widely used (Aun et al., 2021), which however yields a discrete data. Alternatively, automatic chambers can be used but they can alter the local environmental conditions and hinder litter fall (Teramoto et al., 2019), becoming less representative of forest floor. When only few chambers are used, as in this study, also spatial variability may remain unaccounted for. Our study emphasizes that continuous EC measurements at trunk space are an efficient tool to monitor forest floor fluxes (Launiainen et al., 2005; Chi et al., 2021).

To interpret the changes in carbon and water fluxes it is imperative that fluxes are complemented by accurate allometric measurements; this is also necessary to enable the development and benchmarking of forest growth and carbon balance models, and land-surface models to guide future climate-smart and environmentally sustainable forest management. The measurements presented in the study site follows the ICOS protocol for ancillary vegetation measurements (Gielen et al., 2018), which aims to provide standardized measurements with small and similar errors for inter-comparison, setting a good example for future studies. In our study, we showed a significant gradual increase in GPP at forest floor (Fig. 6b). It could however not be verified via the measurements of leaf area, biomass at forest floor, or soil organic carbon.

5. Conclusions

We investigated the short-term effects of commercial thinning (ca. 40% reduction in basal area) on CO_2 and H_2O fluxes in ca. 60 yr old mixed boreal forest with a fully developed canopy structure. The thinning was applied in two stages, i.e. understorey removal and main harvest, with a growing season apart, causing ca. 10 and 35% loss of leaf-area, respectively. This enabled us to study how modification of forest structure affected the fluxes, and how the fluxes recovered during the first two post-thinning years. Understorey removal had no effect on ecosystem gross primary productivity (GPP_{eco}), while increased ecosystem respiration (R_{eco}). The main harvest turned the forest from a long term carbon sink (NEE, −271 g C m^{-2} yr^{-1}) to a moderate source (NEE, + 115 g C m^{-2} yr^{-1}) due to reduced GPP_{eco} and increased R_{eco}. The moderate decrease in GPP_{eco} after the main harvest (ca. 20% compared to the long-term averages) relative to LAI reduction was mainly due to increased light-use efficiency of the remaining trees. Understorey GPP was small after the harvest but steadily increased during the two post-thinning years studied. The decomposition of cutting residue was the main reason of increased R_{eco}, while inter-annual weather variability also played a minor role. The recovery of GPP_{eco} was complete already at the second post-thinning year, while the elevated R_{eco} kept annual NEE (−187 g C m^{-2} yr^{-1}) below the long term averages. Ecosystem ET was more conservative to changes in forest structure, but the ET components at different layers changed. Tree canopy transpiration and interception evaporation decreased, whereas evaporation and transpiration from the forest floor increased due to improved light and water availability and stronger wind speeds.

Our results and extensive literature review showed a strong resemblance in the short-term response of boreal forests to thinning, i.e., reduction in annual photosynthesis, carbon sink, and transpiration. This is likely due to similar management practices and species composition among the studies, and low effect of inter-annual weather variability on fluxes. The model simulations further suggest the relative change in GPP and (evapo)transpiration increase with thinning intensity while being the lower the higher the initial LAI.

Our study demonstrated the advantage of using concurrent above and sub-canopy eddy covariance measurements to disentangle the confounding responses of forest floor and canopy to thinning. Therefore, we recommend implementing the sub-canopy eddy covariance setup in future studies investigating the effects of thinning and other disturbances. We also emphasize the importance of combining process-based modeling and statistical analysis of flux data to better resolve the effect of IAWV and interpret the thinning responses. Our findings improve understanding on forest management footprint in terrestrial carbon and water cycles. When integrated with forest growth and management models, the results promote developing more sustainable and climate-smart forest management practices.

CRediT authorship contribution statement

Toprak Aslan: Writing – review & editing, Writing – original draft, Visualization, Validation, Resources, Project administration, Methodology, Investigation, Funding acquisition, Formal analysis, Data curation, Conceptualization. **Samuli Launiainen:** Writing – review & editing, Writing – original draft, Supervision, Investigation, Conceptualization. **Pasi Kolari:** Data curation, Formal analysis, Investigation, Methodology, Supervision, Writing – original draft, Writing – review & editing. **Olli Peltola:** Writing – review & editing, Formal analysis, Conceptualization. **Juho Aalto:** Writing – review & editing, Writing – original draft, Methodology, Investigation, Formal analysis. **Jaana Bäck:** Writing – review & editing, Funding acquisition. **Timo Vesala:** Writing – review & editing. **Ivan Mammarella:** Writing – review & editing, Writing – original draft, Conceptualization, Data curation, Methodology, Supervision, Validation.

Declaration of competing interest

The authors declare that they have no known competing financial interests or personal relationships that could have appeared to influence the work reported in this paper.

Data availability

The EC fluxes used in the study are available at https://doi.org/10.23729/b4575245-5612-4874-a33b-541b215b1a10 and the auxiliary data at https://doi.org/10.23729/23dd00b2-b9d7-467a-9cee-b4a122486039, latest versions at AVAA – Open research data publishing platform (https://smear.avaa.csc.fi/). The soil chamber data is available at https://b2share.eudat.eu/records/e027118ea22148ef92789e740116711e.The other measured data and the specific dataset and pyAPES model version used in the analysis are available by request from the authors.

Acknowledgments

The study was financially supported by the Research Council of Finland (no. 325680 (BIBIFE), 347780 (ForClimate), 296116 (CLIMOSS), 356138 (LS-HYDRO), 348102 (PREFER), 354298 (PATCHEC), 337549 (ACCC Flagship)), University of Helsinki via ICOS-HY, eLTER FI, EU Horizon 2020 research and innovation programme (no. 871128 (eLTER PLUS)), and the EU Horizon Europe – Framework Programme for Research and Innovation (no. 101056921 (GreenFeedBack), 101059888 (ClimbForest)). TA acknowledges the Vilho, Yrjö, and Kalle Väisälä Foundation for their kind support for funding. Finally, we acknowledge ICOS-RI and ICOS-Finland for funding support, and the SMEAR II staff for maintenance of the long-term research infrastructures.

Appendix A. Filtering criterion for obtaining similar weather conditions

The IAVW and extreme weather conditions can confound the thinning effects if environmental conditions exceptionally vary across pre- and post-thinning years. Thus, when comparing the light and temperature responses of measured fluxes, it is imperative to remove the extreme weather conditions. Accordingly, we constrained measured NEE and ET_{eco} shown in Fig. 7, and measured nighttime respiration of R_{eco}, R_{ff}, and R_{ground} (Appendix C) using T_a, RH, and SWC thresholds. To do so, we (1) pooled T_a, RH, and SWC for each month in growing season covering five years (2018–2022), (2) calculated 0.1 and 0.9 quantiles as thresholds (Table A.5), (3) removed the measured data of interest (i.e., NEE, ET_{eco}) when T_a, RH and SWC were outside the thresholds.

Table A.5
Thresholds of air temperature (T_a in °C), relative humidity (RH in %), and soil water content (SWC) used when filtering measured NEE, ET_{eco}, and respiration (R_{eco}, R_{ff}, R_{ground}). The values inside the brackets represent 0.1 and 0.9 percentiles, respectively.

Variable	May	Jun	Jul	Aug	Sep	Oct
T_a	2.1–18.3	10.2–23.3	11.3–24.9	10.6–21.3	4.8–14.7	−0.6–10.5
RH	29.4–97.3	35.6–92.8	41.2–95.6	48.9–97.3	63.3–99.9	79–100
SWC	0.28–0.32	0.19–0.29	0.16–0.26	0.13–0.24	0.15–0.29	0.19–0.31

Appendix B. Estimation of surface roughness and source area of EC_{eco}

Due to the elevation undulation of the site (Kolari et al., 2022), obtaining singular roughness parameters for the entire forest was challenging. Therefore, we considered only the northern sector (315 < WD and WD < 45), which is more uniform compared to other sectors, for the following analysis. We calculated the aerodynamic roughness length (z_0) and zero-plane displacement height (d) using concurrent 3D (at 27 m) and 2D sonic anemometer (at 33 m) measurements considering the neutral conditions within summer months only (June, July, and August), assuming the validity of the log-linear wind profile near the surface. z_0 was 1.79, 1.87, 2.19, and 1.92 m, while d was 15.8, 15.6, 14.4, and 15 m for 2018–2021, respectively. The increase in z_0 and reduction in d was evident after the main harvest in 2020 and slightly after UR in 2019.

Lindroth et al. (2018) observed similar behavior following a light thinning with 21% BA removal. These findings are also in line with Raupach (1994), who showed a conceptual positive correlation of leaf area with d and a negative correlation with z_0 when the canopy is densely covered with leaves, i.e., one-sided LAI above one.

We calculated the source area of EC_{eco} (defined as 80% of footprint area) following Kljun et al. (2015). The footprint of all studied years was similar, hence, for clarity, we only showed the case in 2018 in Fig. 1a. Interestingly, the change in roughness parameters summarized above resulted in no significant change in flux footprint. This is likely related to the contrasting effect of increasing z_0 that shrinks the footprint and decreasing d that increases the effective measurement height (i.e., measurement height minus d), expanding the footprint. The mean daytime boundaries of the source area were smaller than 150 m, clearly originating from the thinned area (Fig. 1a). The nighttime boundaries were larger due to stable conditions, yet mainly covered the thinned area, only exceeding the thinning area in some cases when wind was from west to south-south west direction . Correspondingly, we consider EC_{eco} fluxes representative and applied no footprint-related filtering.

Appendix C. Partitioning and gap-filling of the eddy covariance data

Eddy covariance technique provides the net exchange of CO_2 (i.e., NEE or NFFE), which is the difference between photosynthetic CO_2 uptake (GPP, μmol m^{-2} s^{-1}) and CO_2 release as respiration (R, μmol m^{-2} s^{-1}). In order to fill the gaps in NEE, and partition it into its components, the NEE/NFFE was approximated by the difference between Eqs. (C.1) and Eq. (C.2), defining R and GPP, respectively:

$$R = R_c Q_{10}^{T/10} \tag{C.1}$$

$$GPP = \frac{\alpha I + GPP_{max} - \sqrt{(\alpha I + GPP_{max})^2 - 4\theta I GPP_{max}}}{2\theta} f(T) \tag{C.2}$$

$$f(T) = -\frac{1}{1 + e^{2(T_0 - T)}} \tag{C.3}$$

where R_c (the base respiration at 10 °C reference temperature), Q_{10} (the factor by which soil respiration increases by a 10 °C increase in temperature), α (–, the canopy light use efficiency), GPP_{max} (μmol m^{-2} s^{-1}, the asymptotic gross photosynthesis rate) and θ (–) are parameters, while I photosynthetic active radiation (μmol m^{-2} s^{-1}), T is temperature (°C). The $f(T)$ is the instantaneous response to air temperature, which follows a sigmoidal shape with an inflection point at T_0 (Kolari et al., 2014).

Using only measured-nighttime NEE and NFFE data, mean of short-term Q_{10} was estimated over two periods, i.e., 2018–2019 and 2020–2022 as 1.53 and 1.65, respectively for EC_{eco}, while one period, i.e., 2019–2022, as 2.3 for EC_{ff}. The mean of air temperature at 16.8 m height and soil temperature at 0.05 m depth was chosen as the driving temperature for EC_{eco}, while the soil organic layer temperature for EC_{ff}. Q_{10} was estimated for moving time windows of 21 days for EC_{eco}, and 31 days for EC_{ff} with 3 days time step. Finally, the mean of the estimated values weighted by the inverse of their confidence intervals was selected for each time period.

The parameters of the GPP model and the base respiration R_c, were estimated using all accepted NEE/NFFE data. The θ was estimated over the period of 2018–2022 as 0.75 for EC_{eco}. The same value was used for EC_{ff}. The PAR_{eco} was used as I for NEE, while PAR_{ff} was used for NFFE. R_c, α, and GPP_{max} were estimated for moving time periods of 11 and 21 days.

The parameters were linearly interpolated to obtain daily values. Later, the continuous time series of GPP and R were constructed using meteorological variables, i.e., PAR and T. For nighttime, R was set

Table C.6
The base respiration at the reference temperature (R_c) of R_{ground}, R_{ff}, R_{eco} for the growing seasons of the study period. The goodness of fit (R^2) is shown within brackets.

	2018	2019	2020	2021	2022
R_{ground}	1.31 (0.89)	1.21 (0.87)	1.12 (0.88)	–	–
R_{ff}	–	0.77 (0.97)	0.77 (0.88)	0.79 (0.92)	0.88 (0.95)
R_{eco}	1.34 (0.94)	1.5 (0.94)	1.56 (0.98)	1.5 (0.98)	1.65 (0.97)

equal to measured NEE/NFFE, while missing values were filled with the complete time series of calculated R. GPP was set to zero. For daytime, GPP overlapping with measured daytime NEE/NFFE was calculated as the difference between modeled R and NEE/NFFE, whereas with missing daytime NEE/NFFE, modeled GPP values were used. When the required driving meteorological variables were missing, NEE/NFFE and the component fluxes were filled by their mean values during the corresponding 30-min period in the time window.

We calculated additional estimates of annual NEE and GPP_{eco} to quantify how much the method selection affects the fluxes. First, we applied the regression method using air temperature as the explanatory variable for ecosystem respiration. Second, we employed REddyProc (Wutzler et al., 2018) with nighttime and daytime partitioning approaches and two different temperatures (air temperature and the mean of air and soil temperatures) for binning NEE and for calculating ecosystem respiration. The meteorological variables were filled before flux partitioning with REddyProc. The turbulence criteria (u_* threshold) for fluxes were the same in all filling and partitioning approaches. The mean NEE and standard deviation among the methods for 2018–2022 was −286 ± 3, −214 ± 8, 132 ± 6, −142 ± 9, −181 ± 4 g C m^{-2} yr^{-1}, respectively. The mean GPP_{eco} and standard deviation for the same period was 1176 ± 7,1200 ± 25, 959 ± 19, 1106 ± 22, and 1220 ± 8, respectively. Thus, the uncertainty of annual fluxes arising from gap-filling and flux partitioning methods is clearly smaller than the observed changes due to thinning.

To investigate the effect of inter-annual weather variability (IAWV) on ecosystem level fluxes in the disturbance years (i.e. 2019 and 2020), we modeled/reconstructed R (R_{eco}) and GPP (GPP_{eco}) via Eqs. (C.1) and (C.2) using the fitting parameters obtained for the 2009–2017 period. The mean daily fitting parameters were used with weather data from 2019–2022, respectively, to compute annual reference flux representing the 'intact forest', and compared with the corresponding year's observed fluxes. The results were shown as cumulative fluxes in Fig. 9. The net fluxes (NEE) were calculated as a difference between R and GPP.

Lastly, in order to assess the possible changes in the base respiration induced by UR and MH in R, we calculated a singular R_c, representing growing season period, for R_{ground}, R_{ff}, and R_{eco}. To do so, we first filtered the data in growing season (following Appendix A) to remove the outliers and to allow a comparison of temperature sensitivities in similar weather conditions across the years. Later, we pooled all available data (2018–2020 for R_{ground}, 2019–2022 for R_{ff}, and 2018–2022 for R_{eco}), then fit Eq. (C.1), resulting in a setup-based Q_{10} of 2.28, 2.32, and 2.36 for R_{ground}, R_{ff}, R_{eco}, respectively. With that, we fit Eq. (C.1) to each growing season data to obtain seasonal R_c, the results of which are summarized in Table C.6, and discussed in Section 4.

References

Aalto, J., Anttila, V., Kolari, P., Ilkka, K., Anna, I., Janne, L., Pauliina, S.-A., Jaana, B., 2023. Hyytiälä SMEAR II forest year 2020 thinning tree and carbon inventory data. http://dx.doi.org/10.5281/zenodo.8138946.

Aubinet, M., Hurdebise, Q., Chopin, H., Debacq, A., De Ligne, A., Heinesch, B., Manise, T., Vincke, C., 2018. Inter-annual variability of net ecosystem productivity for a temperate mixed forest: A predominance of carry-over effects? Agricult. Forest Meteorol. 262, 340–353.

Aun, K., Kukumägi, M., Varik, M., Becker, H., Aosaar, J., Uri, M., Morozov, G., Buht, M., Uri, V., 2021. Short-term effect of thinning on the carbon budget of young and middle-aged Scots pine (Pinus sylvestris L.) stands. Forest Ecol. Manag. 492, 119241.

Aussenac, G., 2000. Interactions between forest stands and microclimate: ecophysiological aspects and consequences for silviculture. Ann. Forest Sci. 57 (3), 287–301.

Balandier, P., Gobin, R., Prévosto, B., Korboulewsky, N., 2022. The contribution of understorey vegetation to ecosystem evapotranspiration in boreal and temperate forests: a literature review and analysis. Eur. J. Forest Res. 1–19.

Baldocchi, D., 2008. 'Breathing'of the terrestrial biosphere: lessons learned from a global network of carbon dioxide flux measurement systems. Aust. J. Bot. 56 (1), 1–26.

Bonan, G.B., 2008. Forests and climate change: forcings, feedbacks, and the climate benefits of forests. Science 320 (5882), 1444–1449.

Brockerhoff, E.G., Barbaro, L., Castagneyrol, B., Forrester, D.I., Gardiner, B., González-Olabarria, J.R., Lyver, P.O., Meurisse, N., Oxbrough, A., Taki, H., et al., 2017. Forest biodiversity, ecosystem functioning and the provision of ecosystem services.

Canadell, J.G., Raupach, M.R., 2008. Managing forests for climate change mitigation. Science 320 (5882), 1456–1457.

Cheng, X., Bai, Y., Zhu, J., Han, H., 2020. Effects of forest thinning on interception and surface runoff in Larix principis-rupprechtii plantation during the growing season. J. Arid Environ. 181, 104222.

Chi, J., Zhao, P., Klosterhalfen, A., Jocher, G., Kljun, N., Nilsson, M.B., Peichl, M., 2021. Forest floor fluxes drive differences in the carbon balance of contrasting boreal forest stands. Agricult. Forest Meteorol. 306, 108454.

Crockford, R., Richardson, D., 2000. Partitioning of rainfall into throughfall, stemflow and interception: effect of forest type, ground cover and climate. Hydrol. Process. 14 (16–17), 2903–2920.

del Campo, A.D., Otsuki, K., Serengil, Y., Blanco, J.A., Yousefpour, R., Wei, X., 2022. A global synthesis on the effects of thinning on hydrological processes: Implications for forest management. Forest Ecol. Manag. 519, 120324.

Dore, S., Kolb, T., Montes-Helu, M., Eckert, S., Sullivan, B., Hungate, B., Kaye, J., Hart, S., Koch, G., Finkral, A., 2010. Carbon and water fluxes from ponderosa pine forests disturbed by wildfire and thinning. Ecol. Appl. 20 (3), 663–683.

Duursma, R.A., Kolari, P., Perämäki, M., Nikinmaa, E., Hari, P., Delzon, S., Loustau, D., Ilvesniemi, H., Pumpanen, J., Mäkelä, A., 2008. Predicting the decline in daily maximum transpiration rate of two pine stands during drought based on constant minimum leaf water potential and plant hydraulic conductance. Tree Physiol. 28 (2), 265–276.

Duursma, R.A., Mäkelä, A., 2007. Summary models for light interception and light-use efficiency of non-homogeneous canopies. Tree Physiol. 27 (6), 859–870.

Foken, T., Babel, W., Munger, J.W., Grönholm, T., Vesala, T., Knohl, A., 2021. Selected breakpoints of net forest carbon uptake at four eddy-covariance sites. Tellus B: Chem. Phys. Meteorol. 73 (1), 1–12.

Foken, T., Wichura, B., 1996. Tools for quality assessment of surface-based flux measurements. Agricult. Forest Meteorol. 78 (1–2), 83–105.

Franz, D., Acosta, M., Altimir, N., Arriga, N., Arrouays, D., Aubinet, M., Aurela, M., Ayres, E., López-Ballesteros, A., Barbaste, M., et al., 2018. Towards long-term standardised carbon and greenhouse gas observations for monitoring Europe's terrestrial ecosystems: a review. Int. Agrophys. 32 (4), 439–455.

Friedlingstein, P., Jones, M.W., O'sullivan, M., Andrew, R.M., Hauck, J., Peters, G.P., Peters, W., Pongratz, J., Sitch, S., Le Quéré, C., et al., 2019. Global carbon budget 2019. Earth Syst. Sci. Data 11 (4), 1783–1838.

Gerten, D., Schaphoff, S., Haberlandt, U., Lucht, W., Sitch, S., 2004. Terrestrial vegetation and water balance—hydrological evaluation of a dynamic global vegetation model. J. Hydrol. 286 (1–4), 249–270.

Gielen, B., Acosta, M., Altimir, N., Buchmann, N., Cescatti, A., Ceschia, E., Fleck, S., Hortnagal, L., Klumpp, K., Kolari, P., et al., 2018. Ancillary vegetation measurements at ICOS ecosystem stations. Int. Agrophys. 32 (4), 645–664.

Granier, A., Bréda, N., Longdoz, B., Gross, P., Ngao, J., 2008. Ten years of fluxes and stand growth in a young beech forest at Hesse, north-eastern France. Ann. Forest Sci. 65 (7), 1.

Grelle, A., Hedwall, P.-O., Strömgren, M., Håkansson, C., Bergh, J., 2023. From source to sink–recovery of the carbon balance in young forests. Agricult. Forest Meteorol. 330, 109290.

Hadden, D., Grelle, A., 2016. Changing temperature response of respiration turns boreal forest from carbon sink into carbon source. Agricult. Forest Meteorol. 223, 30–38.

Härkönen, S., Lehtonen, A., Manninen, T., Tuominen, S., Peltoniemi, M., 2015. Estimating forest leaf area index using satellite images: comparison of k-NN based landsat-NFI lai with MODIS-RSR based LAI product for Finland.

Heikurainen, L., Paivanen, J., et al., 1970. The effect of thinning, clear cutting and fertilization on the hydrology of peatland drained for forestry. Acta Forest. Fennica 104.

Heiskanen, J., Brümmer, C., Buchmann, N., Calfapietra, C., Chen, H., Gielen, B., Gkritzalis, T., Hammer, S., Hartman, S., Herbst, M., et al., 2022. The integrated carbon observation system in Europe. Bull. Am. Meteorol. Soc. 103 (3), E855–E872.

Ilvesniemi, H., Levula, J., Ojansuu, R., Kolari, P., Kulmala, L., Pumpanen, J., Launiainen, S., Vesala, T., Nikinmaa, E., 2009. Long-term measurements of the carbon balance of a boreal Scots pine dominated forest ecosystem. Boreal Environ. Res. 14 (4).

Johansson, M.-B., Berg, B., Meentemeyer, V., 1995. Litter mass-loss rates in late stages of decomposition in a climatic transect of pine forests. Long-term decomposition in a Scots pine forest. IX. Can. J. Bot. 73 (10), 1509–1521.

Katul, G., Grönholm, T., Launiainen, S., Vesala, T., 2010. Predicting the dry deposition of aerosol-sized particles using layer-resolved canopy and pipe flow analogy models: Role of turbophoresis. J. Geophys. Res.: Atmos. 115 (D12).

Keenan, R.J., 2015. Climate change impacts and adaptation in forest management: a review. Ann. Forest Sci. 72, 145–167.

Keenan, R.J., Reams, G.A., Achard, F., de Freitas, J.V., Grainger, A., Lindquist, E., 2015. Dynamics of global forest area: Results from the FAO global forest resources assessment 2015. Forest Ecol. Manag. 352, 9–20.

Kellomäki, S., 2022. Management of Boreal Forests: Theories and Applications for Ecosystem Services. Springer Nature.

Kljun, N., Calanca, P., Rotach, M., Schmid, H.P., 2015. A simple two-dimensional parameterisation for flux footprint prediction (FFP). Geosci. Model Dev. 8 (11), 3695–3713.

Kolari, P., Aalto, J., Levula, J., Kulmala, L., Ilvesniemi, H., Pumpanen, J., et al., 2022. Hyytiälä SMEAR II site characteristics.

Kolari, P., Chan, T., Porcar-Castell, A., Bäck, J., Nikinmaa, E., Juurola, E., 2014. Field and controlled environment measurements show strong seasonal acclimation in photosynthesis and respiration potential in boreal Scots pine. Front. Plant Sci. 5, 717.

Kolari, P., Pumpanen, J., Kulmala, L., Ilvesniemi, H., Nikinmaa, E., Grönholm, T., Hari, P., 2006. Forest floor vegetation plays an important role in photosynthetic production of boreal forests. Forest Ecol. Manag. 221 (1–3), 241–248.

Korkiakoski, M., Ojanen, P., Tuovinen, J.-P., Minkkinen, K., Nevalainen, O., Penttilä, T., Aurela, M., Laurila, T., Lohila, A., 2023. Partial cutting of a boreal nutrient-rich peatland forest causes radically less short-term on-site CO2 emissions than clear-cutting. Agricult. Forest Meteorol. 332, 109361.

Kozii, N., Haahti, K., Tor-ngern, P., Chi, J., Hasselquist, E.M., Laudon, H., Launiainen, S., Oren, R., Peichl, M., Wallerman, J., et al., 2020. Partitioning growing season water balance within a forested boreal catchment using sap flux, eddy covariance, and a process-based model. Hydrol. Earth Syst. Sci. 24 (6), 2999–3014.

Kuuluvainen, T., Tahvonen, O., Aakala, T., 2012. Even-aged and uneven-aged forest management in boreal fennoscandia: a review. Ambio 41, 720–737.

Lagergren, F., Lankreijer, H., Kučera, J., Cienciala, E., Mölder, M., Lindroth, A., 2008. Thinning effects on pine-spruce forest transpiration in central Sweden. Forest Ecol. Manag. 255 (7), 2312–2323.

Launiainen, S., Katul, G.G., Lauren, A., Kolari, P., 2015. Coupling boreal forest CO2, H2O and energy flows by a vertically structured forest canopy – Soil model with separate bryophyte layer. Ecol. Model. 312, 385–405.

Launiainen, S., Katul, G.G., Leppä, K., Kolari, P., Aslan, T., Grönholm, T., Korhonen, L., Mammarella, I., Vesala, T., 2022. Does growing atmospheric CO2 explain increasing carbon sink in a boreal coniferous forest? Global Change Biol. 28 (9), 2910–2929.

Launiainen, S., Rinne, J., Pumpanen, J., Kulmala, L., Kolari, P., Keronen, P., Siivola, E., Pohja, T., Hari, P., Vesala, T., 2005. Eddy covariance measurements of CO2 and sensible and latent heat fluxes during a full year in a boreal pine forest trunk-space. Boreal Environ. Res. 10 (6), 569.

Laurent, M., Antoine, N., Joël, G., 2003. Effects of different thinning intensities on drought response in Norway spruce (Picea abies (L.) Karst.). Forest Ecol. Manag. 183 (1–3), 47–60.

Lemprière, T., Kurz, W., Hogg, E., Schmoll, C., Rampley, G., Yemshanov, D., McKenney, D., Gilsenan, R., Beatch, A., Blain, D., et al., 2013. Canadian boreal forests and climate change mitigation. Environ. Rev. 21 (4), 293–321.

Leppä, K., Korkiakoski, M., Nieminen, M., Laiho, R., Hotanen, J.-P., Kieloaho, A.-J., Korpela, L., Laurila, T., Lohila, A., Minkkinen, K., et al., 2020. Vegetation controls of water and energy balance of a drained peatland forest: Responses to alternative harvesting practices. Agricult. Forest Meteorol. 295, 108198.

Lindner, M., Fitzgerald, J.B., Zimmermann, N.E., Reyer, C., Delzon, S., van Der Maaten, E., Schelhaas, M.-J., Lasch, P., Eggers, J., van Der Maaten-Theunissen, M., et al., 2014. Climate change and European forests: what do we know, what are the uncertainties, and what are the implications for forest management? J. Environ. Manag. 146, 69–83.

Lindroth, A., Holst, J., Heliasz, M., Vestin, P., Lagergren, F., Biermann, T., Cai, Z., Mölder, M., 2018. Effects of low thinning on carbon dioxide fluxes in a mixed hemiboreal forest. Agricult. Forest Meteorol. 262, 59–70.

Lindroth, A., Holst, J., Linderson, M.-L., Aurela, M., Biermann, T., Heliasz, M., Chi, J., Ibrom, A., Kolari, P., Klemedtsson, L., et al., 2020. Effects of drought and meteorological forcing on carbon and water fluxes in nordic forests during the dry summer of 2018. Philos. Trans. R. Soc. B 375 (1810), 20190516.

Ma, S., Concilio, A., Oakley, B., North, M., Chen, J., 2010. Spatial variability in microclimate in a mixed-conifer forest before and after thinning and burning treatments. Forest Ecol. Manag. 259 (5), 904–915.

Mäkelä, A., Kolari, P., Karimäki, J., Nikinmaa, E., Perämäki, M., Hari, P., 2006. Modelling five years of weather-driven variation of GPP in a boreal forest. Agricult. Forest Meteorol. 139 (3–4), 382–398.

Mäkelä, A., Pulkkinen, M., Kolari, P., Lagergren, F., Berbigier, P., Lindroth, A., Loustau, D., Nikinmaa, E., Vesala, T., Hari, P., 2008. Developing an empirical model of stand GPP with the LUE approach: analysis of eddy covariance data at five contrasting conifer sites in Europe. Global Change Biol. 14 (1), 92–108.

Mammarella, I., Launiainen, S., Gronholm, T., Keronen, P., Pumpanen, J., Rannik, Ü., Vesala, T., 2009. Relative humidity effect on the high-frequency attenuation of water vapor flux measured by a closed-path eddy covariance system. J. Atmos. Ocean. Technol. 26 (9), 1856–1866.

Mammarella, I., Peltola, O., Nordbo, A., Järvi, L., Rannik, Ü., 2016. Quantifying the uncertainty of eddy covariance fluxes due to the use of different software packages and combinations of processing steps in two contrasting ecosystems. Atmos. Meas. Tech. 9 (10), 4915–4933.

McJannet, D., Vertessy, R., 2001. Effects of thinning on wood production, leaf area index, transpiration and canopy interception of a plantation subject to drought. Tree Physiol. 21 (12–13), 1001–1008.

Medlyn, B.E., Duursma, R.A., Eamus, D., Ellsworth, D.S., Colin Prentice, I., Barton, C.V., Crous, K.Y., Angelis, P., Freeman, M., Wingate, L., 2012. Reconciling the optimal and empirical approaches to modelling stomatal conductance. Global Change Biol. 18 (11), 3476.

Misson, L., Tang, J., Xu, M., McKay, M., Goldstein, A., 2005. Influences of recovery from clear-cut, climate variability, and thinning on the carbon balance of a young ponderosa pine plantation. Agricult. Forest Meteorol. 130 (3–4), 207–222.

Miura, S., Amacher, M., Hofer, T., San-Miguel-Ayanz, J., Thackway, R., et al., 2015. Protective functions and ecosystem services of global forests in the past quarter-century. Forest Ecol. Manag. 352, 35–46.

Moncrieff, J., Massheder, J., De Bruin, H., Elbers, J., Friborg, T., Heusinkveld, B., Kabat, P., Scott, S., Soegaard, H., Verhoef, A., 1997. A system to measure surface fluxes of momentum, sensible heat, water vapour and carbon dioxide. J. Hydrol. 188, 589–611.

Montagnani, L., Grunwald, T., Kowalski, A., Mammarella, I., Merbold, L., Metzger, S., Sedlák, P., Siebicke, L., 2018. Estimating the storage term in eddy covariance measurements: the ICOS methodology. Int. Agrophys. 32 (4).

Niemistö, P., Kilpeläinen, H., Poutiainen, E., 2018. Effect of first thinning type and age on growth, stem quality and financial performance of a Scots pine stand in Finland. Silva Fennica 52 (2).

Olson, J.S., 1963. Energy storage and the balance of producers and decomposers in ecological systems. Ecology 44 (2), 322–331.

Pan, Y., Birdsey, R.A., Fang, J., Houghton, R., Kauppi, P.E., Kurz, W.A., Phillips, O.L., Shvidenko, A., Lewis, S.L., Canadell, J.G., et al., 2011. A large and persistent carbon sink in the world's forests. Science 333 (6045), 988–993.

Paul-Limoges, E., Wolf, S., Eugster, W., Hörtnagl, L., Buchmann, N., 2017. Below-canopy contributions to ecosystem CO2 fluxes in a temperate mixed forest in Switzerland. Agricult. Forest Meteorol. 247, 582–596.

Paul-Limoges, E., Wolf, S., Schneider, F.D., Longo, M., Moorcroft, P., Gharun, M., Damm, A., 2020. Partitioning evapotranspiration with concurrent eddy covariance measurements in a mixed forest. Agricult. Forest Meteorol. 280, 107786.

Peura, M., Burgas, D., Eyvindson, K., Repo, A., Mönkkönen, M., 2018. Continuous cover forestry is a cost-efficient tool to increase multifunctionality of boreal production forests in Fennoscandia. Biol. Cons. 217, 104–112.

Pinnington, E.M., Casella, E., Dance, S.L., Lawless, A.S., Morison, J.I., Nichols, N.K., Wilkinson, M., Quaife, T.L., 2017. Understanding the effect of disturbance from selective felling on the carbon dynamics of a managed woodland by combining observations with model predictions. J. Geophys. Res. Biogeosci. 122 (4), 886–902.

Prescott, C., Zabek, L., Staley, C., Kabzems, R., 2000. Decomposition of broadleaf and needle litter in forests of British Columbia: influences of litter type, forest type, and litter mixtures. Can. J. Forest Res. 30 (11), 1742–1750.

Priestley, C.H.B., Taylor, R.J., 1972. On the assessment of surface heat flux and evaporation using large-scale parameters. Mon. Weather Rev. 100 (2), 81–92.

Pukkala, T., 2014. Does biofuel harvesting and continuous cover management increase carbon sequestration? Forest Policy Econom. 43, 41–50.

Pukkala, T., Lähde, E., Laiho, O., Salo, K., Hotanen, J.-P., 2011. A multifunctional comparison of even-aged and uneven-aged forest management in a boreal region. Can. J. Forest Res. 41 (4), 851–862.

Pumpanen, J., Kulmala, L., Linden, A., Kolari, P., Nikinmaa, E., Hari, P., 2015. Seasonal dynamics of autotrophic respiration in boreal forest soil estimated by continuous chamber measurements. Boreal Environ. Res. 20 (5), 637.

Rannik, Ü., Vesala, T., 1999. Autoregressive filtering versus linear detrending in estimation of fluxes by the eddy covariance method. Bound.-Layer Meteorol. 91 (2), 259–280.

Raupach, M., 1994. Simplified expressions for vegetation roughness length and zero-plane displacement as functions of canopy height and area index. Bound.-Layer Meteorol. 71 (1), 211–216.

Rebmann, C., Aubinet, M., Schmid, H., Arriga, N., Aurela, M., Burba, G., Clement, R., De Ligne, A., Fratini, G., Gielen, B., et al., 2018. ICOS eddy covariance flux-station site setup: a review. Int. Agrophys. 32 (4), 471–494.

Repola, J., 2008. Biomass equations for birch in Finland.
Repola, J., 2009. Biomass equations for Scots pine and Norway spruce in Finland.
Sabbatini, S., Mammarella, I., Arriga, N., Fratini, G., Graf, A., Hörtnagl, L., Ibrom, A., Longdoz, B., Mauder, M., Merbold, L., et al., 2018. Eddy covariance raw data processing for CO2 and energy fluxes calculation at ICOS ecosystem stations. Int. Agrophys. 32 (4), 495–515.
Saunders, M., Tobin, B., Black, K., Gioria, M., Nieuwenhuis, M., Osborne, B., 2012. Thinning effects on the net ecosystem carbon exchange of a Sitka spruce forest are temperature-dependent. Agricult. Forest Meteorol. 157, 1–10.
Schlesinger, W.H., Jasechko, S., 2014. Transpiration in the global water cycle. Agricult. Forest Meteorol. 189, 115–117.
Skubel, R.A., Khomik, M., Brodeur, J.J., Thorne, R., Arain, M.A., 2017. Short-term selective thinning effects on hydraulic functionality of a temperate pine forest in eastern Canada. Ecohydrology 10 (1), e1780.
Soimakallio, S., Saikku, L., Valsta, L., Pingoud, K., 2016. Climate change mitigation challenge for wood utilization the case of Finland. Environ. Sci. Technol. 50 (10), 5127–5134.
Son, Y., Lee, Y.Y., Jun, Y.C., Kim, Z.-S., 2004. Light availability and understory vegetation four years after thinning in a larix leptolepis plantation of central Korea. J. Forest Res. 9 (2), 133–139.
Song, S., Hu, X., Zhu, J., Zheng, T., Zhang, F., Ji, C., Zhu, J., 2021. The decomposition rates of leaf litter and fine root and their temperature sensitivities are influenced differently by biotic factors. Plant Soil 461, 603–616.
Sun, X., Onda, Y., Otsuki, K., Kato, H., Gomi, T., Liu, X., 2017. Change in evapotranspiration partitioning after thinning in a Japanese cypress plantation. Trees 31 (5), 1411–1421.
Tahvanainen, T., Forss, E., 2008. Individual tree models for the crown biomass distribution of Scots pine, Norway spruce and birch in Finland. Forest Ecol. Manag. 255 (3–4), 455–467.
Tarasov, M.E., Birdsey, R.A., 2001. Decay rate and potential storage of coarse woody debris in the Leningrad region. Ecol. Bull. 137–147.
Teramoto, M., Liang, N., Takahashi, Y., Zeng, J., Saigusa, N., Ide, R., Zhao, X., 2019. Enhanced understory carbon flux components and robustness of net CO2 exchange after thinning in a larch forest in central Japan. Agricult. Forest Meteorol. 274, 106–117.
Thomas, C.K., Martin, J.G., Law, B.E., Davis, K., 2013. Toward biologically meaningful net carbon exchange estimates for tall, dense canopies: Multi-level eddy covariance observations and canopy coupling regimes in a mature Douglas-fir forest in Oregon. Agricult. Forest Meteorol. 173, 14–27.
Venäläinen, A., Lehtonen, I., Laapas, M., Ruosteenoja, K., Tikkanen, O.-P., Viiri, H., Ikonen, V.-P., Peltola, H., 2020. Climate change induces multiple risks to boreal forests and forestry in Finland: A literature review. Global Change Biol. 26 (8), 4178–4196.
Vesala, T., Suni, T., Rannik, Ü., Keronen, P., Markkanen, T., Sevanto, S., Grönholm, T., Smolander, S., Kulmala, M., Ilvesniemi, H., et al., 2005. Effect of thinning on surface fluxes in a boreal forest. Glob. Biogeochem. Cycles 19 (2).
Wilkinson, M., Crow, P., Eaton, E.L., Morison, J.I., 2016. Effects of management thinning on CO2 exchange by a plantation oak woodland in south-eastern England. Biogeosciences 13 (8), 2367–2378.
Wutzler, T., Lucas-Moffat, A., Migliavacca, M., Knauer, J., Sickel, K., Šigut, L., Menzer, O., Reichstein, M., 2018. Basic and extensible post-processing of eddy covariance flux data with REddyProc. Biogeosciences 15 (16), 5015–5030.
Yrjölä, T., 2002. Forest Management Guidelines and Practices in Finland, Sweden and Norway, vol. 11, European Forest Institute Joensuu, Finland.
Zell, J., Kändler, G., Hanewinkel, M., 2009. Predicting constant decay rates of coarse woody debris—a meta-analysis approach with a mixed model. Ecol. Model. 220 (7), 904–912.